MICROCOPY RESOLUTION TEST CHART

NATIONAL BUREAU OF STANDARDS-1963-A

ARO 16881.7.MS

②

NEUTRON DIFFRACTION STUDIES OF SOME

RARE EARTH-TRANSITION METAL DEUTERIDES

FINAL REPORT

William J. James

April 4, 1984

U. S. Army Research Office

DAAG29-80-C-0084

Graduate Center for Materials Research

University of Missouri-Rolla

Rolla; MO 65401

DTIC
ELECTE
MAY 03 1984
S
E
D

APPROVED FOR PUBLIC RELEASE;

DISTRIBUTION UNLIMITED

84   05   01   063

The view, opinions, and/or findings contained in this report are those of the author(s) and should not be construed as an official Department of the Army position, policy, or decision, unless so designated by other documentation.

REPORT DOCUMENTATION PAGE		READ INSTRUCTIONS BEFORE COMPLETING FORM
1. REPORT NUMBER	2. GOVT ACCESSION NO. AD-P140757	3. RECIPIENT'S CATALOG NUMBER
4. TITLE (and Subtitle) NEUTRON DIFFRACTION STUDIES OF SOME RARE EARTH- TRANSITION METAL DEUTERIDES		5. TYPE OF REPORT & PERIOD COVERED Final - 3/15/80 - 11/15/83
		6. PERFORMING ORG. REPORT NUMBER
7. AUTHOR(s) William J. James		8. CONTRACT OR GRANT NUMBER(s) DAAG29-80-C-0084
9. PERFORMING ORGANIZATION NAME AND ADDRESS Graduate Center for Materials Research University of Missouri-Rolla Rolla, MO 65401		10. PROGRAM ELEMENT, PROJECT, TASK AREA & WORK UNIT NUMBERS
11. CONTROLLING OFFICE NAME AND ADDRESS U. S. Army Research Office Post Office Box 12211 Research Triangle Park, NC 27709		12. REPORT DATE April 1984
		13. NUMBER OF PAGES
14. MONITORING AGENCY NAME & ADDRESS(if different from Controlling Office)		15. SECURITY CLASS. (of this report) Unclassified
		15a. DECLASSIFICATION/DOWNGRADING SCHEDULE

16. DISTRIBUTION STATEMENT (of this Report)

Approved for public release; distribution unlimited.

17. DISTRIBUTION STATEMENT (of the abstract entered in Block 20, if different from Report)

NA

18. SUPPLEMENTARY NOTES

The view, opinions, and/or findings contained in this report are those of the author(s) and should not be construed as an official Department of the Army position, policy, or decision, unless so designated by other documentation.

19. KEY WORDS (Continue on reverse side if necessary and identify by block number)

neutron diffraction - magnetic structure - rare earth-transition metal alloys and hydrides

F sub 2   F sub 1

20. ABSTRACT (Continue on reverse side if necessary and identify by block number)

Neutron diffraction studies of the ternary alloy system $Y_6(Fe_{1-x}Mn_x)_{23}$ reveal that the unusual magnetic behavior upon substitution of Mn or Fe into the end members, is a consequence of atomic ordering wherein there is strong site preference of Mn for the f_2 sites and of Fe for the f_1 sites. In the Mn-rich compositions, Fe is found to have no spontaneous moments. Therefore, the long range magnetic ordering arises solely from Mn-Mn interactions. Upon substitution of Mn into the Fe-rich ternaries, the Fe moments are considerably reduced.

20.

Competing antiferromagnetic and ferromagnetic exchange occurs in the $x = 0.4$ to 0.6 range resulting in an absence of long range magnetic order. The phenomenon is similar to that expected of spin-glass behavior. Neutron diffraction studies of $Y_6Mn_{23}D_{23}$ show that a transition occurs below 180K from a fcc structure to a primitive tetragonal structure, space group P4/mmm with the onset of antiferromagnetic ordering. The Mn moments are directed along the c-axis. The transition probably results from atomic ordering of the D atoms at low temperature which induces c axis magnetic ordering. The question of the appropriate space group of $LaNi_{4.5}Al_{0.5}D_{4.5}$, P6/mmm or P3/m has been resolved by a careful refinement and analysis of neutron diffraction data. The preferred space group is P6/mmm. The discrepancy in the space group determination among previous studies appears to arise from a shallow minimum in the profiling function for this system. Neutron powder diffraction and thermal magnetization measurements on small single crystals of $ErNi_3$, $ErCo_3$, and $ErFe_3$ (space group $R\bar{3}m$) show that the magnetocrystalline properties are a consequence of competing local site anisotropies between the two non-equivalent crystallographic sites of Er and two of the three non-equivalent sites of the 3d-transition metal. The Curie temperature of $ErNi_3$ is about 39K. From 39 to about 10K the Er moments are collinear but below 10K there is a reorientation of the spontaneous moment. The moments of Er_I always make an angle with the c-axis smaller than those of Er_{II}. This is consistent with the fact that the easy direction for Er_I is along $\vec{c}$ and for Er_{II} perpendicular to $\vec{c}$. The Curie temperature of $ErCo_3$ is 401K and the magnetic structure is found to be collinear over the temperature range 4.2 - 300K. In effect the Co atoms like the Er_I atoms favor the c-direction and thus the exchange interactions of Er-Co stabilize a collinear array. The Curie temperature of $ErFe_3$ is about 555K. At 4.2K the easy direction is $\vec{c}$ with a spontaneous moment of about 3.74 μ_B/f.u., corresponding to an average moment of about 1.8 μ_B for Fe. At 42K there is a first order magnetic transition from a collinear c-axis structure to a non-collinear one similar to that found for $ErNi_3$. At 300K, a collinear structure is formed with the magnetic moments in the basal plane. At room temperature or above it is evident that the magnetic behavior of $ErFe_3$ arises from the competition among the local anisotropies of the Fe atoms, which by reason of strong exchange interactions, leads to a total anisotropy favoring the basal plane.

Accession For

NTIS GRA&I	☑	
DTIC TAB	☐	
Unannounced	☐	
Justification		

By	
Distribution/	
Availability Codes	
Dist	Avail and/or Special
A-1	

TABLE OF CONTENTS

Page

LIST OF ILLUSTRATIONS

LIST OF TABLES

I. INTRODUCTION

The rare earth hydrides such as RM_3 and R_6M_{23} (where R = rare earth, Y, Th, and M = 3d transition metal) exhibit low plateau pressures at room temperature suggesting their possible use for high power switching devices similar to those employing hydrides of $LaNi_{5-x}Al_x$. Furthermore, the atomic structures of the non-hydrogenated compounds can be related to the RM_2 Laves phase, and the R_2M_{17} and RM_5 phases as instituting building blocks for, say, the RM_3 structure, e.g., $2\ RM_5 - M + R = 3\ RM_3$, also see Fig. 1.

Certain compounds of the latter two structures, R_2M_{17} and RM_5, have been developed with high BH products, e.g., $SmCo_5$. The high magnetocrystalline anisotropy exhibited by such hard magnet materials arises from reinforcement of local site magnetic anisotropies. Accordingly, studies of the magnetic structures of the RM_3 can provide an understanding of how local site symmetries interact to yield the bulk magnetic anisotropy and how these local anisotropies can be altered (by elemental substitution) to provide better magnets.

Additionally, upon hydrogenation the magnetic properties of these intermetallic compounds may change dramatically. As for the RM_3 systems, the magnetic structures of the hydrogenated compounds are relatively unknown; however, in the case of the R_6M_{23} systems, the changes in the magnetic structures of some R_6Mn_{23} compounds are striking upon hydrogenation. Whereas Y_6Mn_{23} exhibits long range magnetic ordering and Th_6Mn_{23} does not, their hydrides exhibit reverse behavior. At low temperatures, < 180K, deuterated Y_6Mn_{23} exhibits antiferromagnetic behavior.

The location of the hydrogen atoms, therefore, not only plays a major role in determining the stability of these hydrides, but also influences their
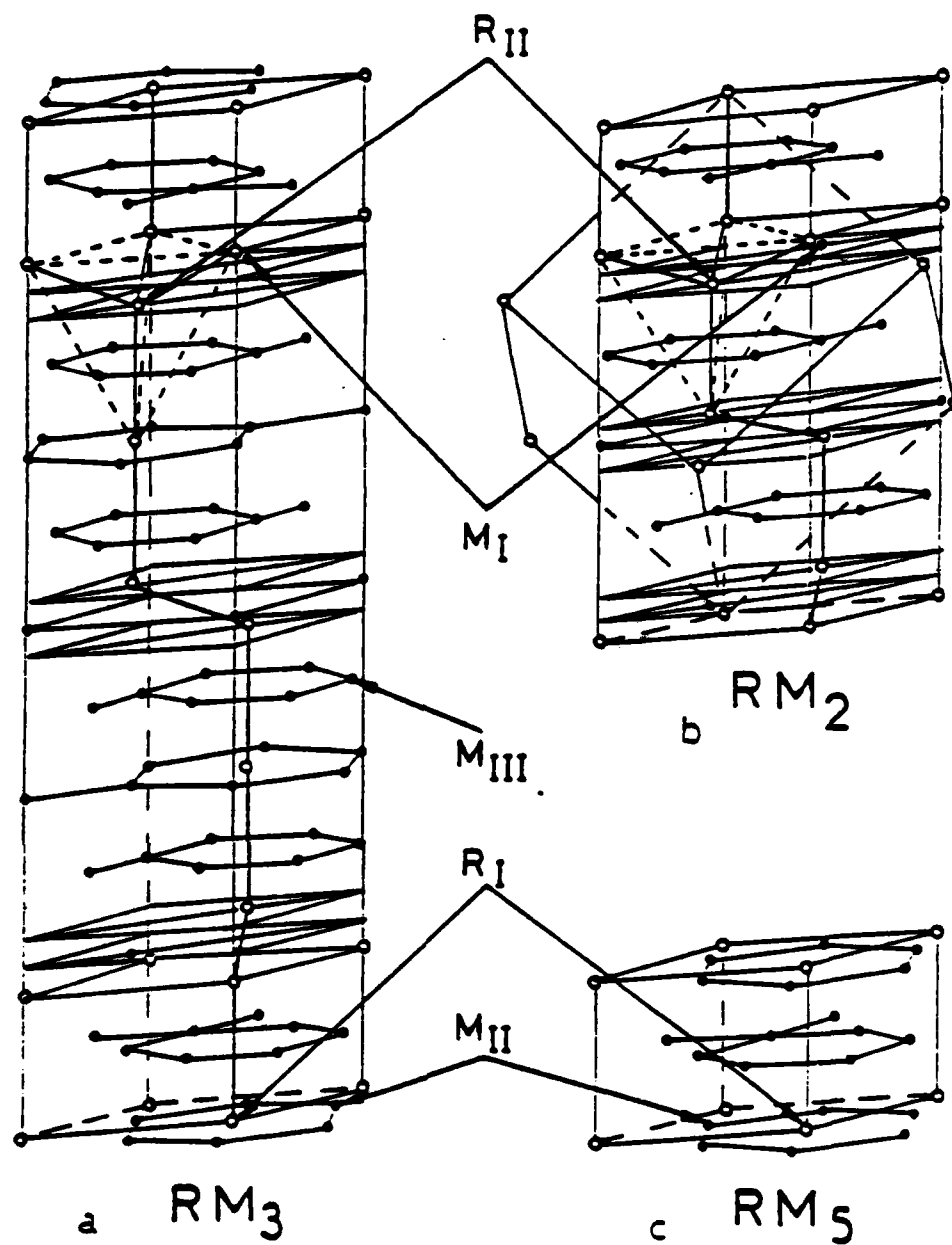
Fig. 1. (a) Crystalline structure of the rhombohedral RM_3 compounds.
         (b) Crystalline structure of the Laves cubic phase RM_2.
         (c) Crystalline structure of the hexagonal RM_5 phase.

electronic and magnetic properties. Neutron diffraction provides a direct means to determining the light atom (deuterium) locations and in addition permits us to determine the extent of atomic ordering when transition metals of neighboring atomic numbers are present in the compounds. In conclusion, neutron diffraction techniques, complemented by magnetic susceptibility measurements and Mössbauer spectroscopy provide a direct probe of magnetic structure and changes therein, possible atomic ordering effects, and site location of the hydrogen (deuterium) atoms.

II. SUMMARY OF RESULTS

A. Magnetic Structures of R_6M_{23} Compounds

1. Y_6Mn_{23} - Effect of Stoichiometric Variations on the Magnetic Moments.
The crystal structure of Y_6Mn_{23} is face centered cubic (Fm3m), isotypical with Th_6Mn_{23}. There are four nonequivalent lattice sites occupied by the Mn atoms and one lattice site (e) occupied by six Y atoms. The four transition metal sites are: b (one atom), d (six atoms), and f_1 and f_2 (eight atoms each). The magnetic structure has been shown[1,2] to be ferrimagnetic with the manganese atoms occupying the four sites, each with its own unique magnetic moment. While these moments are reported to be collinear, the ones on the b and d sites (Wycoff notation) couple antiferromagnetically to those on the f_1 and f_2 sites. The range of values obtained for the individual Mn moments are given in Table I. The results of Hardman et al[1] were obtained using powder neutron diffraction, while those of Delapalme et al[2] were obtained using a single crystal and polarized neutrons. It was suspected that the relatively large variations in the reported Mn moments might arise from large stoichiometric variations between the powders and the single crystal.

Table I. Range of manganese moments for Y_6Mn_{23} reported previously.[1,2]

Site	μ_B per atom at 295 K	μ_B per atom at 4.2 K
Mn_b	2.25 to 3.60	2.81 to 4.34
Mn_d	1.72 to 2.87	2.07 to 2.85
Mn_{f_1}	1.52 to 2.11	1.79 to 2.08
Mn_{f_2}	1.27 to 1.87	1.77 to 2.17

Accordingly, neutron diffraction data were obtained at 80 and 600K for five compositions, Y_6Mn_{21}, Y_6Mn_{22}, Y_6Mn_{23}, Y_6Mn_{24}, Y_6Mn_{25}, and at 9 and 600K for Y_6Mn_{26}. Because some of the ingots contained second phases, these phases had to be subtracted from the neutron patterns before refinement was possible. A previously determined structure for YMn_2[2] was used for calculating relative intensities of expected reflections for this second phase. The appropriate magnitude for this set of calculated reflections was chosen empirically. Calculated gaussian-shaped reflections corresponding to the YMn_2 pattern were then subtracted from the experimentally obtained Y_6Mn_{21} and Y_6Mn_{22} patterns. A similar procedure was used to subtract out YMn_{12} which appeared in the Y_6Mn_{25} and Y_6Mn_{26} patterns. Following the above procedure, the resulting patterns were refined using the Rietveld profiling method.[3]

Atomic absorption analyses showed that the induction melting process was responsible for the evaporation of approximately one formula unit of Mn per stoichiometric unit of compound. High precision, back-reflection, X-ray photographs revealed definite changes in the cell parameters; at room temperature $a_0 = 12.416$Å for Y_6Mn_{21}, and 12.404Å for Y_6Mn_{26}. Similar changes were observed at lower temperatures.

The results of the 80K neutron diffraction pattern refinements are shown in Table II and indicate little change with stoichiometry in the refined crystallographic structure as well as in the refined magnetic moments. The only exceptions are the end members of the stoichiometric range where the moments on the b sites show some variation. Although the Y_6Mn_{26} data were taken at 9K rather than 80K, the Mn moments are essentially saturated at 80K and therefore can still be compared.

Table II. Results of refinements of 80 K data for Y_6Mn_x compounds.[a]

Parameter	Y_6Mn_{21}	Y_6Mn_{22}	Y_6Mn_{23}	Y_6Mn_{24}	Y_6Mn_{25}	Y_6Mn_{26}[b]
Y x coordinate	0.2030(3)	0.2046(2)	0.2047(2)	0.2035(2)	0.2049(2)	0.2046(2)
Mn_f x coordinate	0.1772(2)	0.1774(2)	0.1772(2)	0.1772(2)	0.1776(2)	0.1784(2)
Mn_g x coordinate	0.3787(2)	0.3780(1)	0.3780(2)	0.3776(2)	0.3779(2)	0.3777(2)
Temperature factor (Y)	0.07(6)	0.11(6)	0.10(6)	0.02(5)	−0.08(6)	0.03(9)
Temperature factor (Mn)	0.22(5)	0.09(5)	0.14(5)	0.14(3)	0.17(9)	−0.02(7)
Occupancy (Y)[c]	6.00	6.00	6.00	6.00	6.00	6.00
Occupancy (Mn_b)	0.97(4)	1.02(3)	1.05(3)	1.08(4)	1.07(3)	1.10(4)
Occupancy (Mn_d)	6.08(10)	6.06(7)	6.18(8)	6.21(6)	6.19(6)	6.04(11)
Occupancy (Mn_f)	7.83(12)	8.14(10)	8.33(11)	8.42(10)	8.35(9)	8.42(15)
Occupancy (Mn_g)	8.46(11)	8.06(9)	8.14(10)	8.20(7)	8.16(8)	8.09(7)
μ_B (Mn_b)	−2.4(2)	−3.6(2)	−3.5(1)	−3.5(1)	−3.4(1)	−4.6(2)
μ_B (Mn_d)	−2.0(1)	2.5(1)	−2.4(1)	−2.4(1)	−2.4(1)	−2.5(1)
μ_B (Mn_f)	2.4(1)	1.9(1)	1.9(1)	1.8(1)	1.7(1)	1.9(1)
μ_B (Mn_g)	2.2(1)	1.7(2)	1.8(1)	1.7(1)	1.8(1)	1.7(1)
a_0 (Å)	12.3931(9)	12.4009(3)	12.3975(4)	12.3893(9)	12.3847(9)	12.3825(12)
R factor[d]	6.03	5.06	5.34	5.19	5.26	6.37

[a] Values in parentheses are the standard deviations in the last digit of the expressed parameter.
[b] Data taken at 9 K.
[c] Yttrium occupancy constrained to 6.00 atoms per formula unit.
[d] Weighted profile R factor expressed as a percentage.

It was determined, however, that if small amounts of a second phase are present and not accounted for, the refinement can yield somewhat variable results, particularly for the b site moment. This value is particularly susceptible to such situations because of the low multiplicity[1] of the b site.

It is reasonable, therefore, to conclude that variations in the previously reported moments[1,2] are not a result of major stoichiometric differences in samples. Experimental techniques used in the previous studies are sufficiently precise to reasonably assume a difference of less than one formula unit of Mn per formula unit of Y_6Mn_{23} existed between the two samples. The results presented here clearly show that a stoichiometric difference this small cannot account for the reported differences in magnetic moments.

2. $\underline{Y_6(Fe_{1-x}Mn_x)_{23}}$ - Atomic Ordering and Magnetic Structures. When iron atoms are introduced into the ferrimagnetic compound Y_6Mn_{23}[1], the lattice contracts, the antiferromagnetic Mn-Mn exchange is enhanced which in turn

decreases the magnetization and the Curie temperature. Likewise substitution of Mn into the Y_6Fe_{23} structure lowers the Curie temperature and magnetization but the ensuing changes are drastic and out of proportion to the amounts of substitution, see Fig. 2. For example, in the compositional range x = 0.5 to 0.75, there exists no long range magnetic ordering.[4]
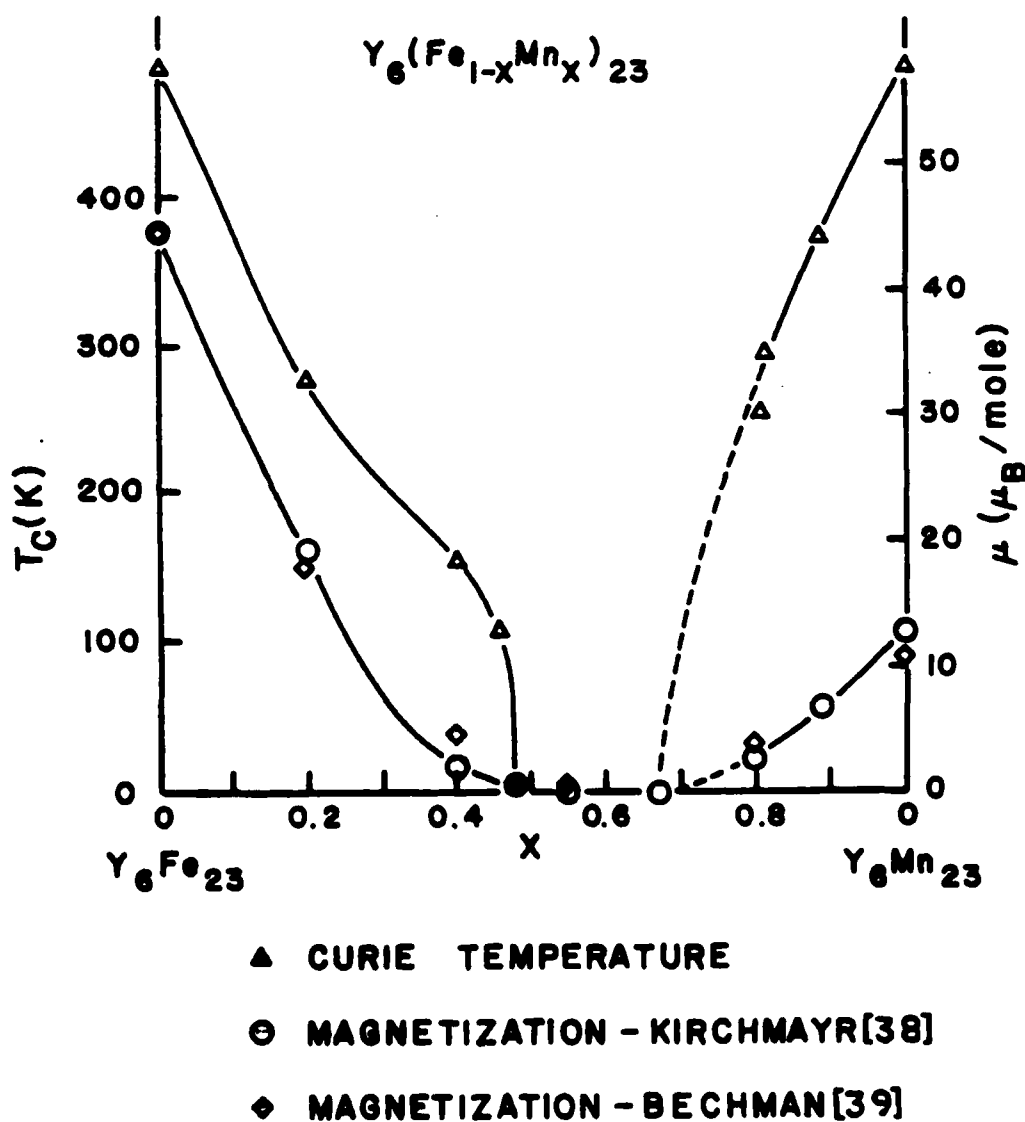
Fig. 2. Curie temperatures and bulk magnetizations for $Y_6(Fe_{1-x}Mn_x)_{23}$ compounds.

Neutron diffraction data were taken on eleven compounds across the compositional range of the system. Substantial preferential ordering of the Fe and Mn atoms occurs with Mn atoms preferring to occupy the f_2 sites and the Fe atoms, the f_1 sites throughout the entire compositional range, Fig. 3.
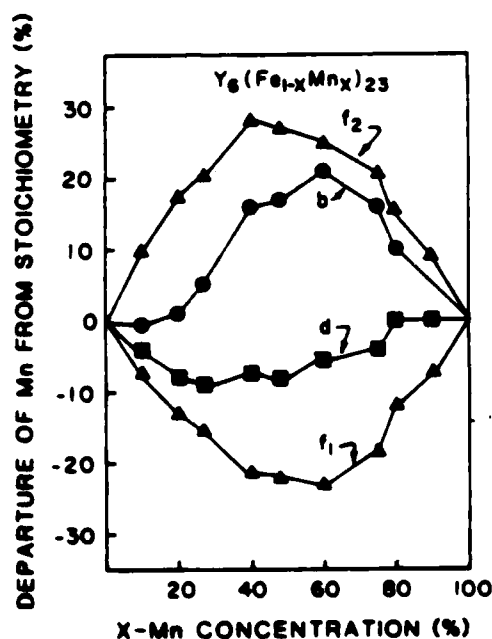
Fig. 3. Preferential site ordering of Mn atoms expressed as a percentage departure from a stoichiometric distribution.

For the Mn-rich compositions (x = 0.8, 0.9, 1.0), the Mn moments on the b and d sites remain coupled antiparallel to those of the two f sites. Mössbauer spectra obtained for x = 0.8 and 0.9 show that the Fe atoms have no spontaneous moment.[5,6] Therefore, the long range magnetic ordering arises solely from the mn-mn substitutions. These interactions, however, are sharply reduced upon the introduction of Fe leading to the pronounced reduced Curie temperatures and magnetizations shown in Fig. 2.

Upon substitution of Mn into the Fe-rich ternaries, the average Fe moments are very much reduced as a consequence of some antiferromagnetic

randomization of Fe and Mn atoms, and thus competing antiferromagnetic and ferromagnetic exchange occurs in the $x = 0.4$ to 0.6 range corresponding to the range of disappearance of long range magnetic order. This frustration phenomenon is similar to that found in many spin-glass systems.

The $Y_6(Fe_{0.73}Mn_{0.27})_{23}$ compound, which is close to the composition at which long range order breaks down, exhibits antiferromagnetic coupling between the Fe moments as opposed to the ferromagnetic coupling observed in the richer Fe ternaries.

3. $\underline{Er_6Mn_{23}}$ - $\underline{Magnetic\ Structure}$. The magnetic structure of this ferrimagnetic structure (T_c = 486K) was determined using powder neutron diffraction (1.8 - 300K), polarized neutron diffraction of a single crystal at 300K, the [111] direction maintained vertical, and from single crystal magnetization measurements along the three principal crystallographic directions [100], [110], and [111].

The polarized neutron results confirm the presence of a collinear structure at 300K. The coupling of the moments on the different Mn sites is the same as observed for Y_6Mn_{23}.[7] The Mn moments in Er_6Mn_{23} are smaller than those in the Y compound; the Er moment is 0.5 μ_B at 300K, Table III.

The magnetization studies show that at 4.2K, [111] is the easy direction of magnetization, but even at $150KO_e$, saturation is not achieved. Magnetization measurements along [100] and [110] reveal a large magnetocrystalline anisotropy. Above 100K the anisotropy disappears, and a large susceptibility is superposed upon the spontaneous magnetization.

All observed reflections of the neutron powder data are characteristic of the Th_6Mn_{23} structure. Only slight variations are observed in the intensities of the different reflections between 300 and 100K. Below 100K there is a pronounced change in the intensities resulting mainly from the magnetic

9

Table III. Thermal variation of Er and Mn moments.

	Y_6Mn_{23}		Er_6Mn_{23}		
	4.2K*	300K*	300K*	100	4.2
R	--	--	.50 (5)	1.35 (6)	7.5 (1)
Mn_1 (4b)	-2.81 (12)	-2.25 (9)	-1.88 (9)	-2.5 (2)	-2.6 (2)
Mn_2 (24d)	-2.07 (4)	1.72 (4)	-1.44 (4)	-1.6 (1)	-1.7 (1)
Mn_3 ($32f_1$)	1.79 (4)	1.52 (3)	1.21 (4)	-1.6 (1)	1.6 (1)
Mn_4 ($32f_2$)	1.77 (4)	1.27 (3)	1.05 (3)	-1.5 (1)	1.5 (1)

*polarized neutron diffr. () standard deviation.

contributions of the Er atoms. A collinear model does not give a satisfactory fit to the neutron data. At 4.2K the best fit results in a noncollinear model retaining the same Mn sub-lattice as found for Y_6Mn_{23} but with lower moment values. The Er moments are inclined at $\theta = 9°$ from the cube axis on which the Er atom lies. The Er moment is 7.5 μ_B, considerably less than the free ion value ($g_J\mu_B = 9$ μ_B). The thermal variation of the Er moment and its angle with the cube axis is shown in Fig. 4.
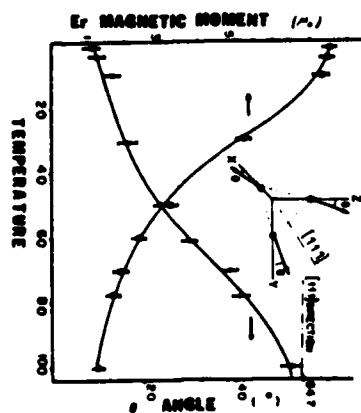
Fig. 4. Variation of $|M_{Er}|$ and θ (angle of M_{Er} to [100]) with temperature.

The Curie temperatures of Er_6Mn_{23} and Y_6Mn_{23} are of the same order of magnitude indicating the Mn-Mn interactions to be dominant; they stabilize the strong ferrimagnetic coupling of the Mn sites. In the Mn compounds the coupling between Mn atoms is very sensitive to the distance of separation. Due to the lanthanide contraction, the Mn-Mn distances are smaller for the Er compound than for Y_6Mn_{23}; accordingly, there is a slight decrease of Curie temperature and therefore smaller Mn moments for the former.

The magnetic configuration of Er atoms is a result of crystal field and exchange field effects on the Er moments. As a consequence of the special position of the Er atoms on the cube axis, there results an axial local symmetry. The second order terms of the crystal field are, therefore, dominant. In the Stevens notation, the Hamiltonian of an Er atom is given by

$$H = s\mu_B H_{ex} + \alpha_J V_2^0 0_2^0$$

where α_J is the Stevens coefficient, 0_2^0 is a crystal field operator, and V_2^0 characterizes the electrical environment of the rare earth atom. $\alpha_J V_2^0$ is negative in Er_6Mn_{23}. At low temperatures the crystal field term favors the [100] direction. The Er atoms on the three different cube axes have easy directions normal to each other, thus the magnetic structure is noncollinear.

The rotation of the Er moments is not associated with a transition between two configurations of nearly equal energy. Rather, it results from the temperature effect on the crystal field levels in the presence of the exchange field. This result is consistent with our specific heat measurements which show no anomaly.

We have attempted to fit the variation of the spontaneous magnetization along [111] with the temperature (300 - 100K) using $H_{ex} = 30k0_e$.[8] The best fit is obtained for $\alpha_J V_2^0 = 1.2K$.

B. Atomic and Magnetic Structures of Hydrides

1. $Y_6Mn_{23}D_{23}$ - Structural and Magnetic Properties. The magnetic behavior of Y_6Mn_{23} is dramatically altered upon hydrogenation (or deuteration). For example, it has been reported[9] that Th_6Mn_{23} is a Pauli paramagnet whereas $Th_6Mn_{23}H_{23}$ is ferromagnetic with $T_c = 355K$. By contrast, Y_6Mn_{23} is ferrimagnetic whereas $Y_6Mn_{23}D_{23}$ shows no net spontaneous magnetization, even at 4.2K.[9] In an attempt to explain the effect of hydrogenation, powder neutron diffraction data were collected at 298 and 80K on the two-axis neutron diffractometer at the Missouri University Research Reactor. Refinement of the data was carried out using a Rietveld profile technique as modified by Prince.[10] Magnetic susceptibilities were measured by the extraction method at the Service Nationale des Champs Intenses at Grenoble, France. Measurements were performed at temperatures from 2 to 300K and at fields up to 150 kOe.

The initial refinement of neutron data at room temperature assumed a face-centered cubic symmetry as used in an earlier study.[11] Results of the refinement of room temperature data showed deuterium atoms occupying the 4a, $32f_3$, 96j, and 96k sites (Wycoff notation) as shown in Table IV. The 96j and 96k sites were significantly less than fully occupied. The refined cell parameter was found to be 12.789Å, slightly less than that reported by Commandre et al,[12] but in good agreement with the 12.78Å obtained by Buschow and Sherwood[13] using X-ray diffraction. Other parameters agreed fairly well with those obtained by Commandre et al[12] and by Hardman and Rhyne,[14] the only exception being the variable coordinate of the Y site which was in better agreement with the results of the latter group. The refinement gave a

Table IV. Results of room temperature structure determinations of $Y_6Mn_{23}D_{23}$ using face-centered cubic symmetry.

Site	Position	Parameter	a	b	c
Y 24e	x,0,0	N	6	6	6
		x	.235	.208	.210(1)
Mn 4b	½,½,½	N	1	1	1
Mn 24d	0,¼,¼	N	6	6	6
Mn 32f$_1$	x,x,x	N	8	8	8
		x	.186	.182	.183(1)
Mn 32f$_2$	x,x,x	N	8	8	8
		x	.377	.370	.375(1)
D 4a	0,0,0	N	1	1	1
D 32f$_3$	x,x,x	N	8	5.6	8.4(3)
		x	.101	.102	.103(1)
D 96j	0,y,z	N	9.6	9	10.4(4)
		y	.167	.167	.157(2)
		z	.370	.373	.366(2)
D 96k	x,x,z	N	4.3	6.4	3.7(3)
		x	.153	.16	.161(2)
		z	.011	.046	.043(2)
cell parameter (Å)		a$_o$	12.840		12.789(3)
R-factor			4.8%		5.8%
R-profile (weighted)					9.9%
R-expected					4.8%

(a) M. Commandre, et al. [22], (b) K. Hardman and J. J. Rhyne [26], (c) present study.

weighted profile R-factor of 9.9% and a best expected R-factor of 4.8% yielding a X-value (defined as the weighted profile R-factor divided by the best expected R-factor) of 2.1.

Data taken at 80K showed the presence of new peaks not present at room temperature. These new reflections could only be explained by an ordered

array of magnetic moments. No report of this existed previous to this study. The new reflections could only be indexed by reducing the overall symmetry. A probable choice for the reduced symmetry was body-centered tetragonal. At this stage the questions arose as to whether this resulting distortion (reduction in cubic symmetry) occurred as magnetic ordering took place or upon deuteration of Y_6Mn_{23}.

Accordingly, the room temperature data were again refined based on a structure having I4/mmm symmetry, see unit cell, Fig. 5. The large square is the original cubic unit cell, the smaller canted square is the tetragonal unit cell. In the tetragonal cell the Y atoms occupy the 4e and 8h positions while Mn atoms occupy the 2b, 4c, 8f, $16n_1$, and $16n_2$ sites. Results of the refinement yielded a weight profile R-factor of 6.4% and a X value of 1.8 which was significantly better than that obtained using fcc symmetry.

Returning to the magnetic refinement of the 80K data, in as much as there was no bulk magnetization evidenced by the compound, any magnetic ordering had to be antiferromagnetic in nature. Furthermore, our susceptibility measurements were characteristic of antiferromagnetic behavior, Fig. 6. A Néel transition temperature of about 160K was evidenced by the cusp in the susceptibility plot. The linear nature of the plots with temperature, and at all applied fields from 5 to 150 kOe indicated the Mn-Mn interactions to be strong.

The absence of 00ℓ reflections in the neutron diffraction pattern at 80K suggested a collinear magnetic structure with the moments aligned parallel to the c-axis of the tetragonal cell. However, due to the time reversal symmetry elements (or antisymmetry elements) that occur in magnetic systems as a consequence of reversal of moment directions when spin and orbital motions are reversed, the body centered tetragonal symmetry had to be reduced to primitive

14
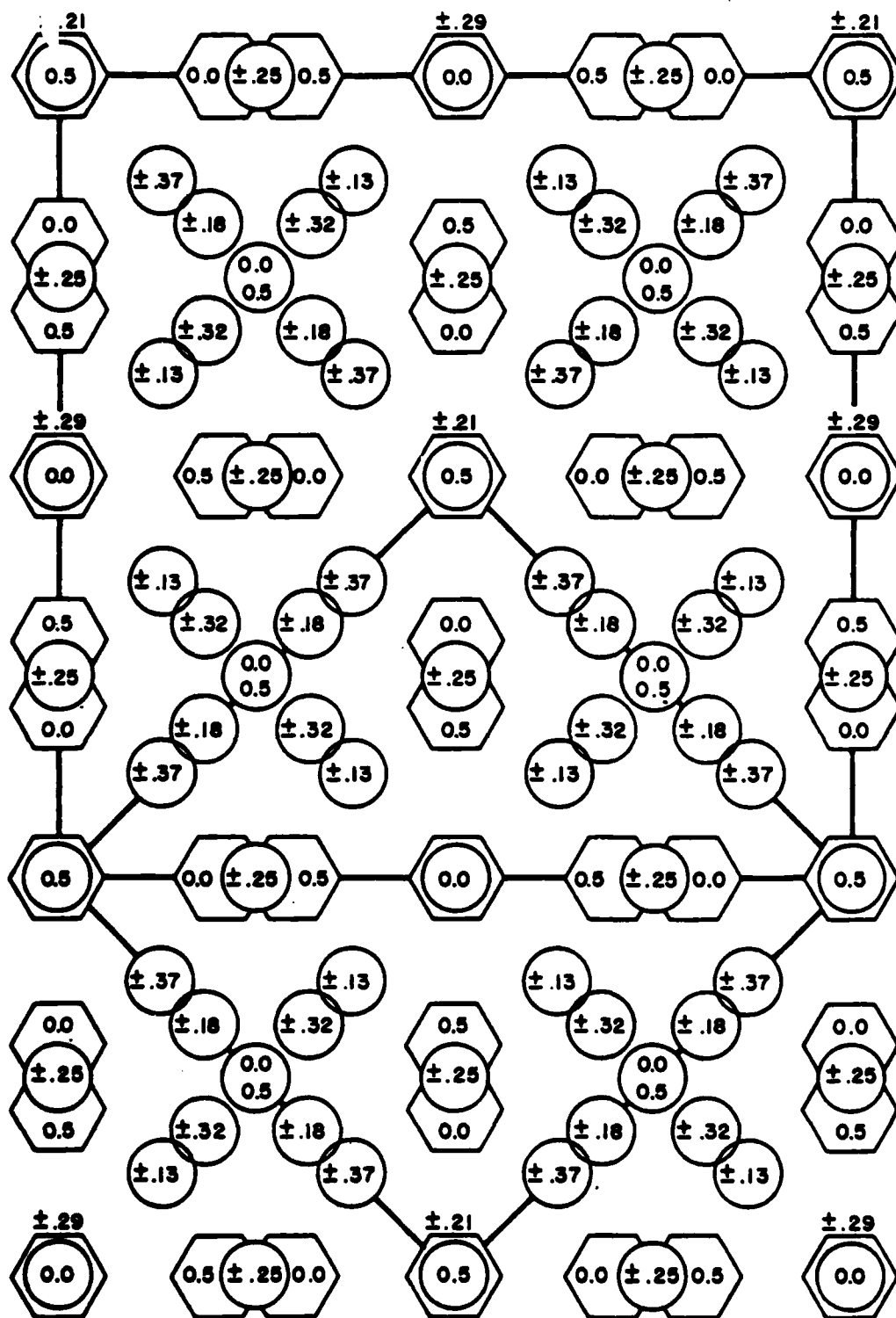
Fig. 5. Cubic and tetragonal unit cells for the Th_6Mn_{23} structure.

tetragonal P_4/mmm, or, in terms of a "Shubnikov" space group, $P_I4/mm'm'$. Refinement resulted in a magnetic R-factor of about 16% which was considered somewhat high in that the overall χ value for both atomic and magnetic ordering was in excess of 2.5.

Below 80K, the magnetic susceptibility was observed to rise slowly with decreasing temperature, see Fig. 6. This could not be explained by a simple antiferromagnetic model. Accordingly, we decided to collect additional neutron diffraction data in collaboration with Kay Hardman-Rhyne and J. J. Rhyne at NBS using their high-resolution five-detector powder diffractometer.

At 295K the NBS data, taken over a wider scattering angle range with a higher instrumental resolution, indicated no departure from fcc symmetry for $Y_6Mn_{23}D_{23}$. The structural parameters were derived from a modified Rietveld refinement based on the space group Fm3m, see Table V. The deuterium atoms were found to prefer the a, f_3, j_1, and k_1 sites. Based on geometric model criteria[15] that hydrogen atoms cannot be closer together than 2.1Å, the j_1 site cannot have more than 12 deuterium atoms per formula unit. Ten deuteriums per formula unit were found. The model also predicts that deuterium atoms cannot occupy the k_1 site unless some deuterium atoms are removed from the f_3 site. This was indeed found to be the case, in contrast to that of Commandre et al[12] who reported the f_3 site filled and four deuterium atoms in the k_1 site.

The temperature factors for deuterium in the a and j_1 sites are quite large suggesting for the a site that there is little or no bonding to the six Y atoms surrounding it. As for the j_1 site, the high thermal factor probably arises from an averaging effect of D atoms, disordered between two j_1 sites that are only 0.90Å from one another.

Table V. Equivalent positions in two crystallographic space groups. $Z = 4$ for the Fm3m structure, and $Z = 2$ for the P4/mmm structure.

	Face-centered cubic ($Fm\,3m$)			Primitive tetragonal ($P4/mmm$)					
atom	site	x,y,z	$N/2$ f.u.	site	x,y,z	x	y	z	$N/2$ f.u.
Y	e	$x,0,0$	12	g	$0,0,z$			0.205	2
		$x=0.205$		h	$\frac{1}{2},\frac{1}{2},z$			0.295	2
				j	$x,x,0$	0.205			4
				k	$x,x,\frac{1}{2}$	0.295			4
Mn	b	$\frac{1}{2},\frac{1}{2},\frac{1}{2}$	2	b	$0,0,\frac{1}{2}$				1
				c	$\frac{1}{2},\frac{1}{2},0$				1
Mn	d	$0,\frac{1}{4},\frac{1}{4}$	12	e	$0,\frac{1}{2},\frac{1}{2},$				2
				f	$0,\frac{1}{2},0$				2
				r_1	x,x,z	0.25		0.75	8
Mn	f_1	x,x,x	16	s_1	$x,0,z$	0.358		0.179	8
		$x=0.179$		t_1	$x,\frac{1}{2},z$	0.142		0.321	8
Mn	f_2	x,x,x	16	s_2	$x,0,z$	0.256		0.372	8
		$x=0.372$		t_2	$x,\frac{1}{2},z$	0.244		0.128	8
D	a	$0,0,0$	2	a	$0,0,0$				1
				d	$\frac{1}{2},\frac{1}{2},\frac{1}{2},$				1
D	f_3	x,x,x	16	s_3	$x,0,z$	0.200		0.100	8
		$x=0.100$		t_3	$x,\frac{1}{2},z$	0.300		0.400	8
D	j_1	$0,y,z$	48	p	$x,y,0$	0.204	0.458		8
		$y=0.169$		q	$x,y,\frac{1}{2}$	0.296	0.042		8
		$z=0.373$		r_2	x,x,z	0.127		0.331	8
				r_3	x,x,z	0.169		0.373	8
				r_4	x,x,z	0.331		0.127	8
				r_5	x,x,z	0.373		0.169	8
D	k_1	x,x,z	48	s_4	$x,0,z$	0.322		0.049	8
		$x=0.161$		t_4	$x,\frac{1}{2},z$	0.178		0.451	8
		$z=0.049$		u_1	x,y,z	0.112	0.210	0.161	16
				u_2	x,y,z	0.290	0.388	0.339	16

A crystallographic distortion is evidenced below 180K as shown in the expanded high angle data for $Y_6Mn_{23}D_{23}$ at 295 and 4K, Fig 7. In the 4K data at $2\theta = 91.0°$, the (11,3,3) and (9,7,3) reflections have split and the intensities have changed. In the fcc lattice at 295K there is only one peak observed in this region.

18
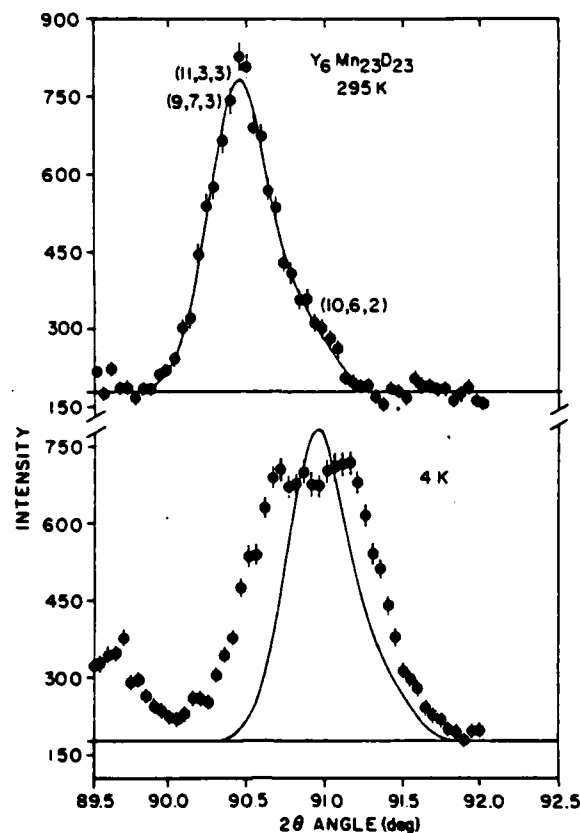
Fig. 7. Expanded high angle data for $Y_6Mn_{23}D_{23}$ at 295 and 4K showing the peak broadening accompanying the tetragonal distortion below the crystal structure transition temperature. Solid lines in both cases are the profile fit for the 295K fcc data. Shift in the solid line represents the lattice contraction at low temperatures.

The best fit to the nuclear structure of $Y_6Mn_{23}D_{23}$ at low temperatures (T < 180K) is P4/mmm. This structure, as shown in Table V, splits the single e site into four sites (g, h, j, k) and the b site into b and c sites. The d site is split into e, f, and r sites. The Mn f site and the Df site are split into s and t sites. The Da site is split into a and d sites, and the Dj site is split into p, q, and four r sites.

Only half of the original (fcc) j site can be filled. The results, Table VI, show the p site to be half filled, the q site almost half filled, and the r_2, r_4 sites almost filled. There are no D atoms in the r_3 and r_5 sites. The

Table VI. Atomic parameters of $Y_6Mn_{23}D_{23}$ at 78 and 4K in the P4/mmm tetragonal structure. All x, y, z, and B values were refined except the x, y, z values that are 0 or . All deuterium occupancy values were also refined.

atom	site	N (max)	78 K				4 K			
			x	y	z	B	x	y	z	B
Y	g	2 (2)	0	0	0.208	0.76	0	0	0.213	0.72
	h	2 (2)	$\frac{1}{2}$	$\frac{1}{2}$	0.287	0.76	$\frac{1}{2}$	$\frac{1}{2}$	0.285	0.72
	j	4 (4)	0.199	0.199	0	0.76	0.204	0.204	0	0.72
	k	4 (4)	0.291	0.291	$\frac{1}{2}$	0.76	0.297	0.297	$\frac{1}{2}$	0.72
Mn	b	1 (1)	0	0	$\frac{1}{2}$	0.25	0	0	$\frac{1}{2}$	0.01
	c	1 (1)	$\frac{1}{2}$	$\frac{1}{2}$	0	0.25	$\frac{1}{2}$	$\frac{1}{2}$	0	0.01
Mn	e	2 (2)	0	$\frac{1}{2}$	$\frac{1}{2}$	0.25	0	$\frac{1}{2}$	$\frac{1}{2}$	0.01
	f	2 (2)	0	$\frac{1}{2}$	0	0.25	0	$\frac{1}{2}$	0	0.01
	r_1	8 (8)	0.259	0.259	0.748	0.25	0.255	0.255	0.747	0.01
Mn	s_1	8 (8)	0.360	0	0.177	0.25	0.360	0	0.182	0.01
	t_1	8 (8)	0.135	$\frac{1}{2}$	0.318	0.25	0.145	$\frac{1}{2}$	0.317	0.01
Mn	s_2	8 (8)	0.277	0	0.379	0.25	0.275	0	0.387	0.01
	t_2	8 (8)	0.250	$\frac{1}{2}$	0.129	0.25	0.249	$\frac{1}{2}$	0.137	0.01
D	a	1 (1)	0	0	0	6.12	0	0	0	7.80
	d	1 (1)	$\frac{1}{2}$	$\frac{1}{2}$	$\frac{1}{2}$	5.16	$\frac{1}{2}$	$\frac{1}{2}$	$\frac{1}{2}$	7.90
D	s_3	4.7(8)	0.217	0	0.095	1.21	0.219	0	0.093	0.25
	t_3	5.3(8)	0.305	$\frac{1}{2}$	0.398	0.02	0.305	$\frac{1}{2}$	0.398	0.02
D	p	4 (8)	0.204	0.464	0	4.55	0.230	0.438	0	2.30
	q	3 (8)	0.291	0.072	$\frac{1}{2}$	1.48	0.304	0.045	$\frac{1}{2}$	1.80
	r_2	6 (8)	0.138	0.138	0.338	3.04	0.141	0.141	0.331	2.83
	r_3	(8)								
	r_4	7 (8)	0.351	0.351	0.131	4.35	0.360	0.360	0.132	2.40
	r_5	(8)								
D	s_4	2.5(8)	0.322	0	0.077	0.40	0.324	0	0.041	1.08
	t_4	(8)								
	u_1	3.5(16)	0.073	0.174	0.166	3.30	0.066	0.177	0.141	2.67
	u_2	8 (16)	0.299	0.385	0.333	0.16	0.296	0.392	0.327	0.20

k site splits into s_4, t_4 and two u sites. No more than nine D atoms/f.w. can fill these sites. Table VI shows the t_4 site to be empty.

As regards the magnetic structure, the neutron data show new peaks emerging in the 2θ range from 20.0 to 21.5°, at temperatures between 165 and 178K. Analysis of the data at 78 and 4K reveals a weak antiferromagnetic structure with only two sites of the original fcc structure participating in

the long range order, Table VII. The Mn moments are directed along the c-axis. The splitting of the f sites allows the Mn atoms to be divided among two sites (s and t) with antiparallel moments which correspond to antiferromagnetism on the equivalent fcc site. The d and the f_1 sites of the fcc structure appear to have no magnetic moment. Larger moments on the f_2 sites were found for $Y_6Mn_{23}D_{23}$ at 78K rather than at 4K. This corresponds to the broad minimum observed at about 80K in the magnetic susceptibility, Fig. 6.

Table VII. Magnetization values in μ_B/Mn atom for Y_6Mn_{23} and $Y_6Mn_{23}D_{23}$. Negative and positive signs indicate directions of the magnetic moments of the Mn atoms.

		P4/mmm structure					Fm3m structure	
$Y_6Mn_{23}D_{23}$		78 K	4 K	$N/2$ f.u.	Y_6Mn_{23}		4 K	$N/2$ f.u.
Mn	b	−3.60	−3.68	1	Mn	b	−3.05	2
	c	+3.60	+3.68	1				
Mn	e	0	0	2	Mn	d	−2.34	12
	f	0	0	2				
	r_1	0	0	8				
Mn	s_1	0	0	8	Mn	f_1	+1.99	16
	t_1	0	0	8				
Mn	s_2	+2.08	+1.60	8	Mn	f_2	+1.80	16
	t_2	−2.08	−1.60	8				
	a_0	9.031	9.030			12.402		
	c_0	12.723	12.722					
	Z=2					Z=4		
	R_{wp}	9.97	8.64			8.38		
	R_e	6.06	5.81			4.34		
	$\chi = R_{wp}/R_e$	1.64	1.49			1.93		

To summarize, the room temperature structure for $Y_6Mn_{23}D_{23}$ is fcc with space group Fm3m. The deuterium atoms fill the a site and partially fill the f_3, j_1, and k_1 sites which is in reasonable agreement with the Westlake model[15] for $A_6B_{23}H_x$ compounds.

There is a structural and accompanying magnetic transition occurring at about 175K. The crystal structure transforms to a primitive tetragonal space group P4/mmm. This transformation probably results from the atomic ordering of the D atoms at low temperature which induces the c axis antiferromagnetic

21

ordering on the Mn sites. $Y_6Mn_{23}D_{23}$ is only weakly antiferromagnetic with the Mn atoms on the b and f_2 sites having finite magnetic moments, which, in the tetragonal phase, corresponds to Mn moments on the b and t_2 sites coupled antiparallel to those on the c and s_2 sites. No ordered moment was found on the Mn d and f_1 sites of the fcc structure.

2. $\underline{LaNi_{4.5}Al_{0.5}D_{4.5} - Structure~at~298~and~77K}$. In the study of magnetic intermetallic compounds, it is important that an accurate determination of space group and atomic structure be made, particularly if the atomic moment directions and magnitudes are to be determined. With hydrides, or with compounds involving metals of nearly similar atomic numbers, X-rays are not sufficient for structure determinations. These structures are often solved using neutron diffraction and Rietveld profiling. Although this study deals with a non-magnetic hydride, the principles involved are applicable to other hydrides of the $CaCu_5$-type intermetallics which are magnetic.

$LaNi_5$ has a hexagonal crystal structure belonging to the P6/mmm space group.[16] Whereas $LaAl_5$ does not exist, Al may be substituted for Ni up to a composition of about $LaNi_{3.5}Al_{1.5}$.[17] Studies of the crystallographic structures of these hydrides[18,19] have resulted in conflicting reports, particularly over the space group symmetry. Percheron-Guegan et al[18] maintain that the hydrides have structures belonging to the P6/mmm space group, suggesting that the metal atom positions are essentially unchanged upon hydrogenation. The hydrogen atoms are reported to be in five distinct crystallographic locations. Fischer and co-workers[19] contend that the structure of the $LaNi_5$ hydride belongs to the P3/m space group. Others[20] have also reported this structure. This model indicates that the metal atoms have been shifted slightly from their highly symmetric positions during

hydrogenation. The hydrogen atoms are reported to be in only two crystallographic locations. Both studies have been carried out at room temperature.

More recently, Wallace et al[21] have calculated configurational entropies for the two reported structures. These values were compared with an experimental value derived from heat capacity measurements made by Ohlendorf and Flotow[21] for $LaNi_5H_{6.39}$. The P3/m structure gave a configurational entropy close to the thermodynamically derived value, whereas the structure reported by Percheron-Guegan gave a configurational entropy three times that of the experimental value.

NMR data reported by Barnes et al[22] appear to support the P3/m structure whereas NMR data reported by Halstead[23] appear to support the P6/mmm structure.

Therefore, we undertook to determine the structure of $LaNi_{4.5}Al_{0.5}H_x$ where x was determined to be 4.5. Powder neutron diffraction data were taken at 298 and 77K on the two-axis diffractometer at the University of Missouri Research Reactor. Careful analysis of the Rietveld profiling results were used to determine the structure and its temperature dependence. Each pattern was analyzed twice--once using P6/mmm symmetry and then using P3/m symmetry. The results, Table VIII, indicate very little difference in R-factors between the two models. However, it is noteworthy that the metal atom coordinates reported by Fischer et al for P3/m structure have moved upon refinement to values one standard deviation or less distant from the coordinates given by the P6/mmm model.

The discrepancy in space group determination among previous studies appears to arise from a shallow minimum in the profiling function for this system. Five coordinates among the atoms are affected by the space group

23

Table VIII. Refinement results for $LaNi_{4.5}Al_{0.5}D_{4.5}$, 298K data.

Atom	P6/mmm Site	Positional Parameters	(a)	(b)
La	1a	x,y,z	0.0	0.0
Ni	2c	z	0.0	0.980(9)
Ni	3g	x	0.5	0.485(5)
		z	0.5	0.495(5)
Ni	6	x	0.290	0.270*
		y	0.580	0.540*
		z	0.0	0.02 *
Ni	2e	z	0.310	0.290*
Al	3g	x	0.5	0.485(5)
		z	0.5	0.495(5)
D	6m	x	0.139	0.155(20)
		y	0.861	0.836(18)
		z	0.5	0.508(16)
D	6i	x	0.5	0.490(9)
		z	0.120	0.090(7)
R-profile (weighted)			4.11%	4.53%

Refined Composition

$P6/mmm$ -- $La_{0.91}Ni_{4.50}Al_{0.50}D_{4.43}$

$P31m$ -- $La_{0.90}Ni_{4.50}Al_{0.50}D_{4.72}$

(a) P6/mmm symmetry with two deuterium sites.
(b) P31m symmetry with two deuterium sites.
 * The occupation of these sites is too small to obtain meaningful standard deviations.

choice. These are the z coordinate of the 2c Ni site (2b in P3/m), the x and z coordinates of the 3g Ni-Al site (3c in P3/m), and z coordinate of the 6m D site (6d in P3/m), and the x coordinate of the 6i D site (3c in P3/m). Fischer reported these coordinates as 0.94, 0.47, 0.48, 0.56, and 0.47, respectively,

whereas in the P6/mmm space group these coordinates are specified as 0.0, 0.5, 0.5, 0.5, and 0.5, respectively. A series of eight profile analyses were carried out in which these coordinates were constrained at values ranging from slightly more displaced that those of Fischer through the symmetrical P6/mmm values. The resulting R factors are given in Table IX and illustrated graphically in Fig. 8a. The broad, shallow minimum is quite evident in this region, Fig. 9.

The same series of analyses was carried out for the 77K data. The results which are very similar to the room temperature series are illustrated in Fig. 8b and the refined positional parameters given in Table X. At the lower temperature there is a decided improvement in the profile fit to the neutron data using the 2 site P6/mmm symmetry, R factor of 3.73 as opposed to 6.68 for the P3/m symmetry. The cell length, a, shows a contraction from 5.341 to 5.331Å, while c remains at 4.236Å.

The discrepancy between the configurational entropy calculated from the structure reported by Achard et al[18] and the experimentally derived value arises primarily from the abundance of fractionally filled hydrogen sites. The two site model results in a calculated configurational entropy that is lower and in better agreement with experiment. The configurational entropy is calculated from the expression; $S_c = k \ln W$, where W is the number of complexations associated with distributing n times N_0 atoms of deuterium over m times N_0 sites. W is derived from the following expression:

$$W = \frac{(\alpha m N_0)!}{(n N_0)! \cdot \{(m-n)N_0\}!}$$

Table IX. Dependence of R-factors on displacement of atom positions for $LaNi_{4.5}Al_{0.5}D_{4.5}$.

Refinement no. --	1	2	3*	4	5	6	7**	8
z (2c Ni site)	0.910	0.925	0.940	0.955	0.970	0.985	0.000	0.015
z (3g Ni-Al site)	0.470	0.475	0.480	0.485	0.490	0.495	0.500	0.505
z (3g Ni-Al site)	0.4550	0.4625	0.4700	0.4775	0.4850	0.4925	0.5000	0.5075
z (6m D site)	0.590	0.575	0.560	0.545	0.530	0.515	0.500	0.485
x (6i D site)	0.4550	0.4625	0.4700	0.4775	0.4850	0.4925	0.5000	0.5075
R-factor*** (298 K)	12.56	9.80	7.82	5.97	5.12	5.20	5.19	9.97
R-factor*** (77 K)	13.15	10.04	7.27	6.30	5.28	5.20	5.31	5.96

* These values correspond to the structure reported by Fischer et al. [4].

** These values correspont to P6/mmm symmetry.

*** These are the weighted profile R-factors expressed in percent.

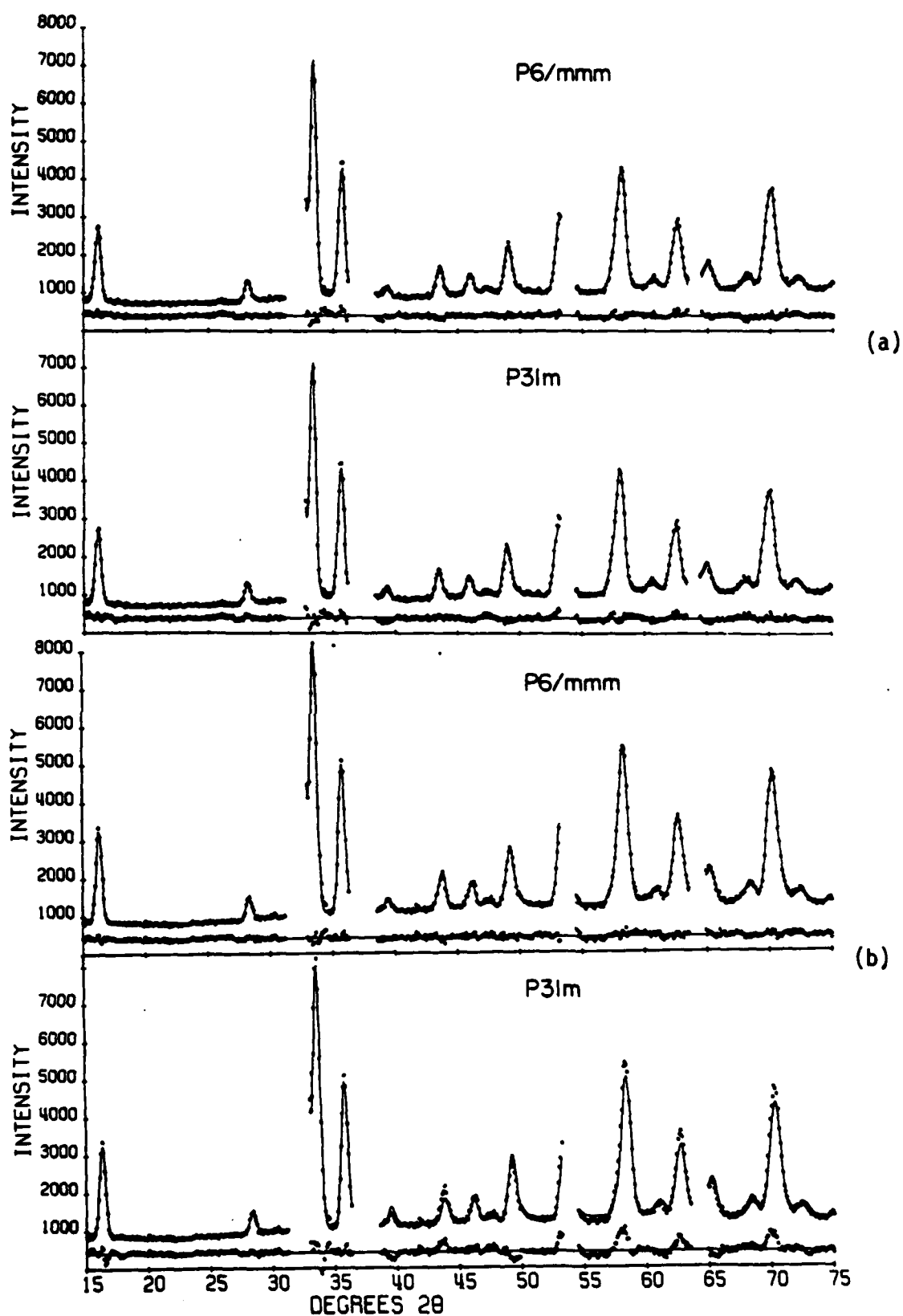26

Fig. 8. Data and refined patterns for LaNi$_{4.5}$Al$_{0.5}$D$_{4.5}$: (a) at room temperature, and (b) at 77K.
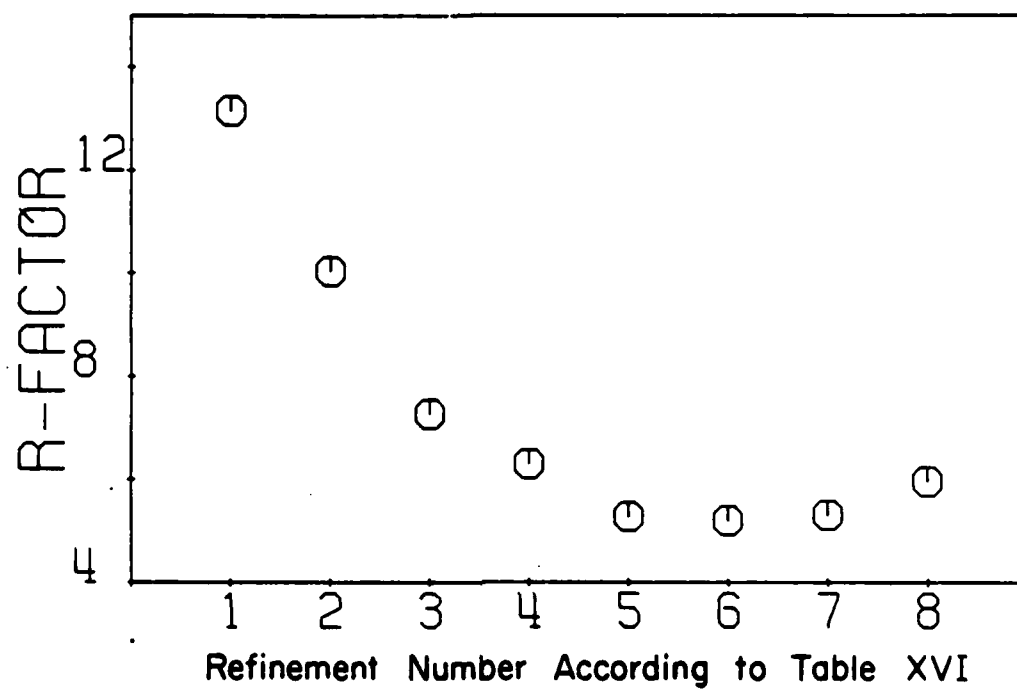
Fig. 9. The effect of atom position on the R-factor for
$LaNi_{4.5}Al_{0.5}D_{4.5}$ refinements at room and 77K temperature.

Table X. Refinement results for $LaNi_{4.5}Al_{0.5}D_{4.5}$, 77K data.

Atom	P6/mmm Site	Positional Parameters	(a)	(b)
La	1a	x,y,z	0.0	0.0
Ni	2c	z	0.0	0.965(12)
Ni	3g	x	0.5	0.480(8)
		z	0.5	0.478(14)
Ni	6	x	0.290	0.270*
		y	0.580	0.540*
		z	0.0	0.02 *
Ni	2e	z	0.310	0.290*
Al	3g	x	0.5	0.480(8)
		z	0.5	0.478(14)
D	6m	x	0.140	0.164(30)
		y	0.860	0.840(28)
		z	0.5	0.511(28)
D	6i	x	0.5	0.485(15)
		z	0.103	0.070(14)
R-profile (weighted)			3.73%	6.68%

(a) P6/mmm symmetry with two deuterium sites.
(b) P31m symmetry with two deuterium sites.
 * The occupation of these sites is too small to
   obtain meaningful standard deviations.

where m is the multiplicity of the site, α is the fraction of this multiplicity of sites that can actually be occupied without atomic overlap, and n is the actual occupation number. This two-site model results in a calculated configurational entropy of 6.1 J/°K mole H, compared to an experimentally derived value for $LaNi_5H_{6.39}$ of 4.3 J/°K mole H. It is presumably valid to compare these values as the experimental ΔS values for hydriding these compounds are practically identical.[24] The calculated configurational entropy for Fischer's P3/m structure is 5.4 J/°K mole H while that for Achard's P6/mmm structure is 11.3 J/°K mole.

Thus, the neutron data indicate that the symmetry is P6/mmm while the entropy values show that a two-site hydrogen model for the structure is preferrable over a five-site model. This latter conclusion is also supported by the neutron data. The fact that a trigonal (6i) site is occupied, rather than a tetrahedral (12n) site is indicative of the high mobility of the deuterium atoms within the metal lattice. While the lowest energy configuration is most likely one with atoms in the (12n) positions, the amplitude of the deuterium atom vibration is quite high and compares with the (12n) - (12n) intersite distance. Thus these atoms are continually making jumps from one (12n) site to the next. The trigonal (6i) site is an energy saddle point midway between these (12n) sites and the deuterium atoms would be moving much slower when passing through these sites than through the (12n) sites. Even if the deuterium atom did not contain quite enough energy to make the jump, it would still be spending much more time at the ends of its vibrational movements near the (6i) sites than at the (12n) equilibrium positions. Thus the time averaged neutron diffraction "picture" sees the atoms in the (6i) positions. This phenomenon explains why the kinetics of the hydrogen absorption and desorption for $LaNi_{4.5}Al_{0.5}D_{4.5}$ are much faster than

30

those for $Y_6Mn_{23}D_{23}$ or $Er_6Mn_{23}D_{23}$, where all deuterium atoms are confined to tetrahedral or octahedral sites and are not observed in any trigonal "saddle point" sites.

C. Neutron Diffraction and Magnetic Studies of ErM_3 Intermetallics

1. $ErNi_3$ - Magnetization Measurements and Magnetic Structure. With the exception of $CeNi_3$, the rare earth-nickel compounds of this stoichiometry crystallize in the rhombohedral structure of $PuNi_3$, space group $R\overline{3}m$. As previously mentioned, these structures can be deduced from the structure of the RM_5 compounds by means of appropriate ordered substitutions of rare earth atoms for transition metal atoms,[25] e.g.,

$$2MR_5 - M + R = 3RM_3 = R_I2R_{II}M_I2M_{II}6M_{III}$$
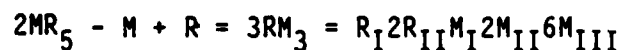
· Examination of Fig. 1 reveals that the rare earth atoms are restricted to two crystallographic sites: R_I which has an environment of nearest neighbor atoms nearly that of the rare earth in the RM_5 structure; and R_{II} corresponding to the rare earth in the substitution zone with an environment nearly that of a rare earth atom in the cubic Laves phase. This latter phase can be also derived from the RM_5 structure by the same substitutions which generated the RM_3 compounds, namely

$$RM_5 - M + R = 2RM_2$$

In the Laves phase the one crystallographic site of the rare earth has a cubic symmetry corresponding to $\overline{4}3m$ and as a consequence the nearest neighbor environment of the R_{II} atom in the RM_3 structure is a slightly distorted tetrahedron, with elongation occurring parallel to the $\overline{3}$ axis.

The transition metal atoms are distributed over three sites where two, M_I and M_{II}, have axial symmetry, with the third, M_{III}, having planar symmetry. M_I

31

has the same environment as M atoms in the Laves phase and M_{II} the same as in the RM_5 phase, see Table XI.

Table XI. Atom positions for the rhombohedral RM_3 intermetallics (+ rhombohedral translations).

Atoms	Site	Positions	
3 R_I	3a	$(0,0,0)$	
6 R_{II}	6c	$\pm(0,0,z)$	$z = 0.141$
3 M_I	3b	$(0,0,\frac{1}{2})$	
6 M_{II}	6c	$(0,0,z)$	$z = 0.333$
18 M_{III}	18h	$\pm(x,\bar{x},z);\pm(x,2x,z);$ $\pm(2\bar{x},\bar{x},z)$	
		$x = 0.509$	$z = 0.082$

A single crystal of $ErNi_3$ was grown by the Czochralski method in the Néel laboratory in Grenoble, France where the magnetization studies were performed. Figs. 10a and b show several magnetization isotherms versus applied field along the c and b axes. As the temperature increases, the magnetization at zero field in the basal plane decreases rapidly and vanishes at 10K. Above this temperature, the zero field magnetization along the c axis corresponds to the spontaneous moment; the c axis has become the easy axis of magnetization. The spontaneous moment vanishes at about 39K, the Curie temperature. Accordingly, there is a reorientation of the spontaneous moment below 10K. At 4.2K the spontaneous magnetization makes an angle of about 29° with the c axis.

As the crystal was too small for neutron diffraction, the neutron data were collected at temperatures of 4.2 to 25K on powders prepared at Rolla and

32
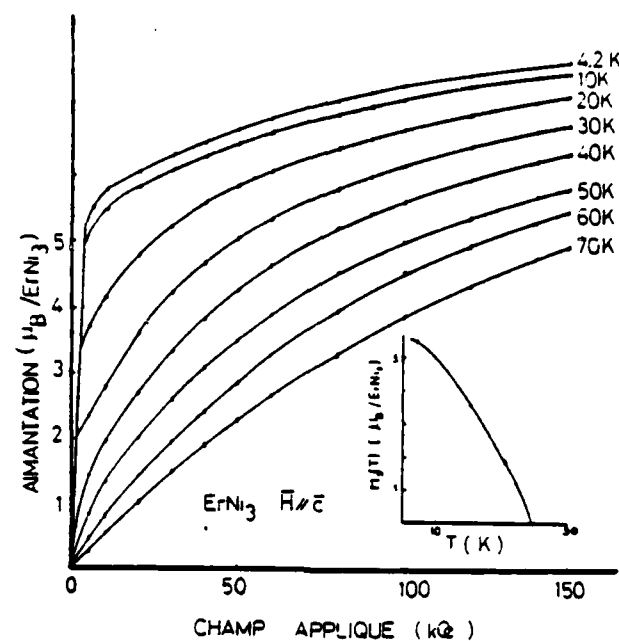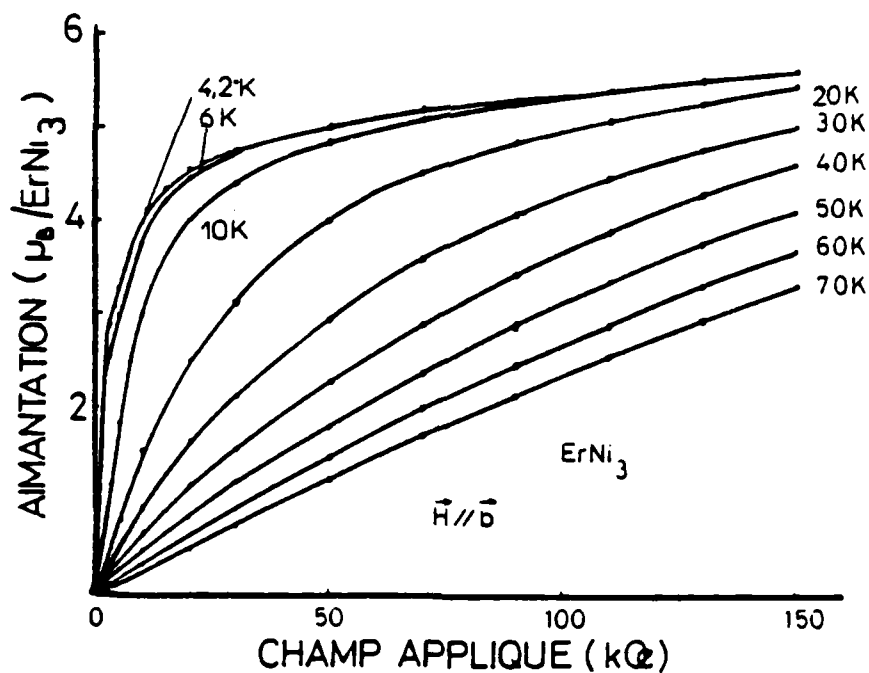
Fig. 10. Magnetization isotherms versus applied field for ErNi₃:
(a) $\vec{H}$ parallel to $\vec{c}$, and (b) $\vec{H}$ parallel to $\vec{b}$.

33

that of the atomic periodicity, i.e., no evidence of an
ordering.

Between 10 and 25K there was no evidence of (003),
indicating the magnetic axis to be collinear along the c axis
moments were determined from Rietveld refinement of the neutro
given in Table XII. Below 10K strong (00ℓ) peaks were evident
refinement indicated the magnetic structure to be noncollinear;
the two Er atoms are in the same plane containing the c axis.
and the angles (θ) the moments make with the c axis are giver
The weighted R factors are all of the order of 3%.

Table XII. Neutron diffraction results at 4.2, 5.5, 10, and 25

T(K)	4.2	5.5	10	
Er_I $M(\mu_B)$	8.5 ± 0.8	8.4 ± 0.4	6.3 ± 0.4	4
θ_I	$10 \pm 5°$	$5 \pm 4°$	$0°$	
Er_{II} $M(\mu_B)$	7.5 ± 0.5	5.3 ± 0.2	3.4 ± 0.2	1
	$55 \pm 5°$	$24 \pm 4°$	$0°$	

The noncollinear structure below 10K is in accord with th
$ErNi_3$ at 4.2K by Yakinthos et al.[26] Our data reveal the
increasing temperature to a collinear structure. The represe
magnetic moments undoubtedly results from competition betw

34

anisotropies of the magnetic atoms coupled through exchange. Since in $ErNi_3$ the magnetism of Ni is negligible, this competition in anisotropies results from the two different environments of the Er atoms. The moments of Er_I always make an angle with the c axis smaller than those of Er_{II}. This is consistent with the fact that the easy direction for Er_I is along $\vec{c}$ and for Er_{II} it is perpendicular to $\vec{c}$, as inferred from Fig. 1. The evolution with temperature toward a collinear structure parallel to $\vec{c}$ arises from the more rapid decrease of the local anisotropy of the Er_{II} atoms.

2. $\underline{ErCo_3 - Magnetization\ Measurements}$. The Curie temperature of $ErCo_3$ is about 401K.[27] The magnetization isotherms as a function of applied field along the a, b, and c axes are shown in Figs. 11a and b. It is evident that the c axis is the easy direction with a spontaneous moment of about 5 μ_B for $ErCo_3$ assuming the moments of Co to be 1.33 μ_B/Co, as in $GdCo_3$. A moment of 9 μ_B/Er results which corresponds to the maximum $gJz\mu_B$ and the magnetic structure is thus collinear. In contrast to $ErNi_3$ no evidence of reorientation of the easy axis was observed over the temperature range 4.2-300K. In effect the cobalt atoms like the Er_I atoms favor the c direction and the exchange interactions of Er-Co stabilize a collinear array.

When the field is applied perpendicular to the c-axis, the magnetization curves exhibit a sharp change for a critical value of field, Figs. 10a and b. At 4.2K this critical field, Hc, attains values of 23 and 21 kOe along the b and a directions, respectively. The critical field increases with increasing temperature although the amplitude (ΔM, μ_B/$ErCo_3$) of the dicontinuity decreases. Beyond the critical field, the magnetization is less than the spontaneous magnetization.

3. $\underline{ErFe_3 - Magnetization\ Measurements\ and\ Magnetic\ Structure}$. The Curie temperature of $ErFe_3$ is about 555K.[28] Figs. 12a and b give the result of

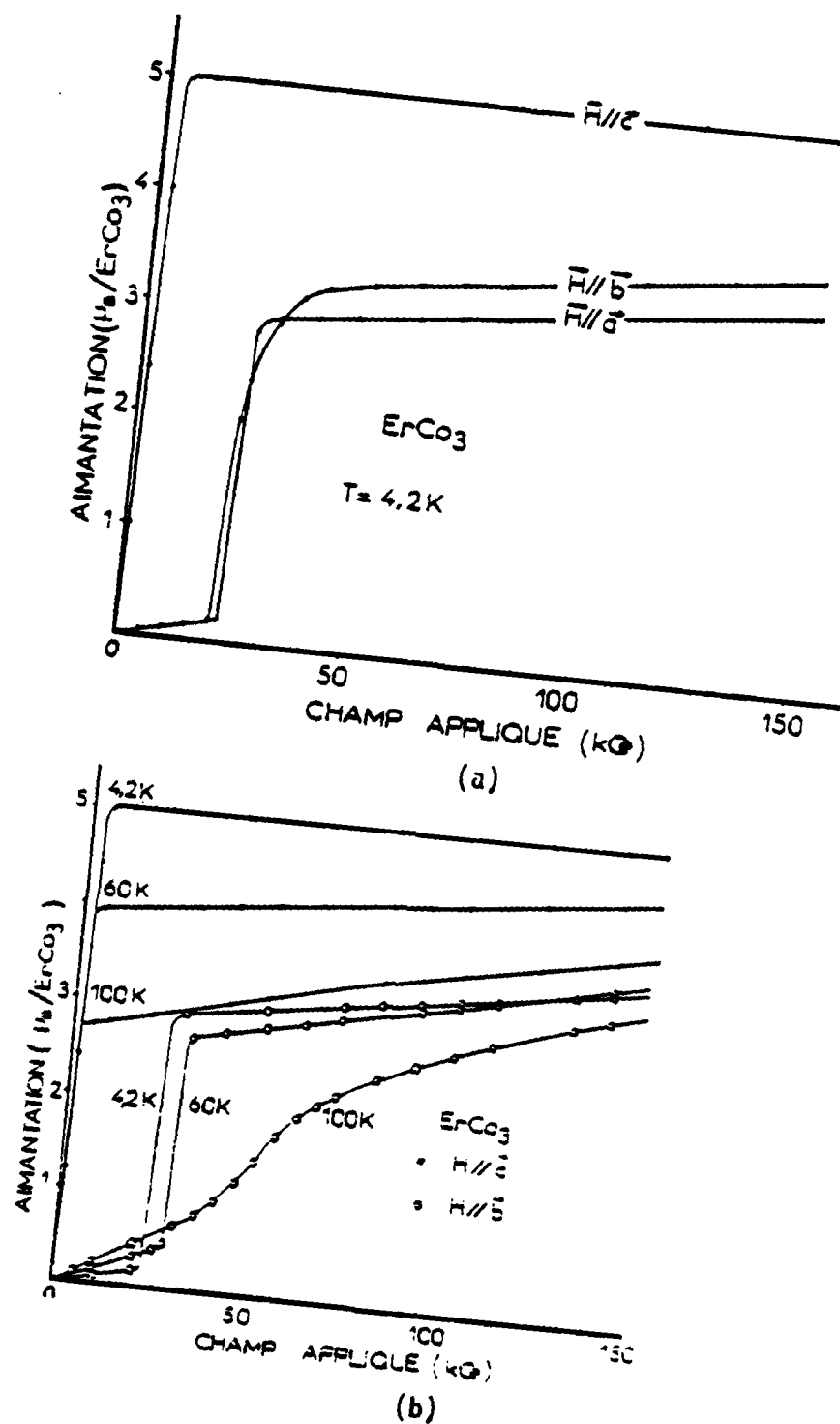35

Fig. 11. Magnetization isotherms versus applied field for $ErCo_3$:
(a) $\vec{H}$ parallel to $\vec{a}$, $\vec{b}$, $\vec{c}$ at 4.2K, and (b) $\vec{H}$ parallel to
$\vec{b}$ and $\vec{c}$ at various temperatures.

36
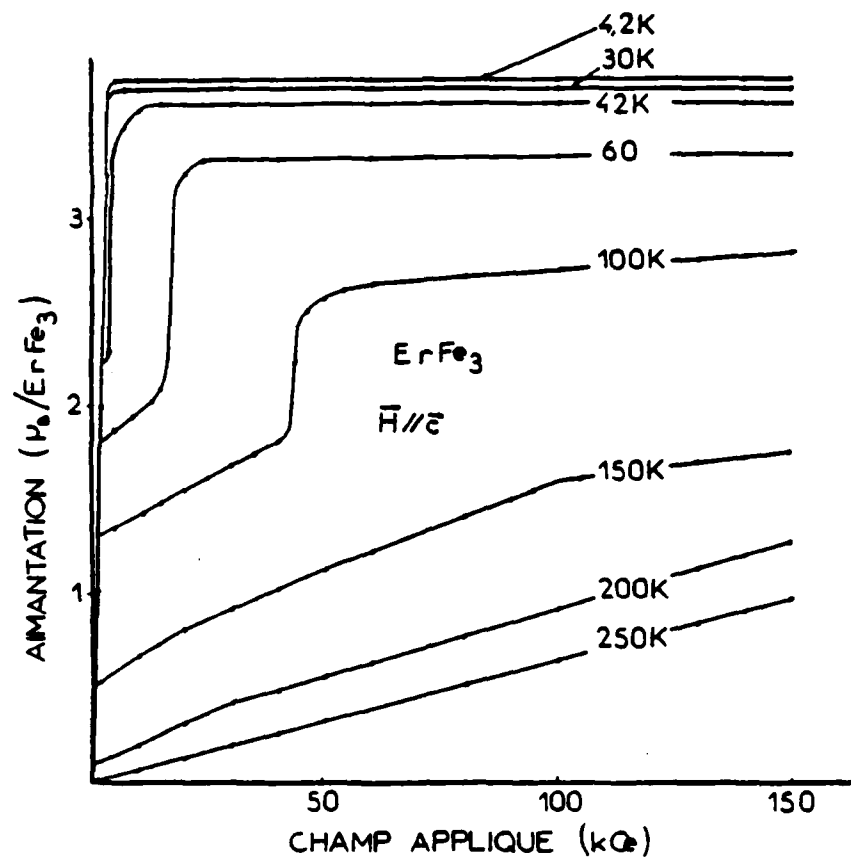
(a)
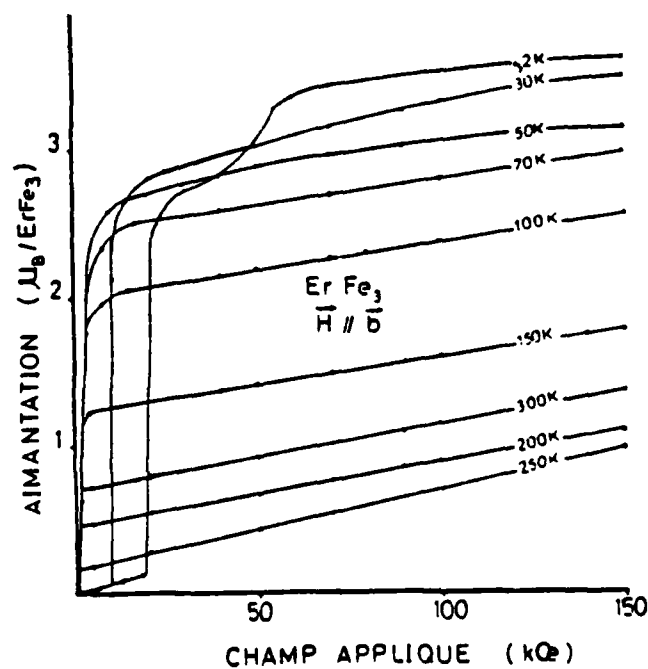
(b)

Fig. 12. Magnetization isotherms versus applied field at various
temperatures for ErFe$_3$: (a) $\vec{H}$ parallel to $\vec{c}$, and (b) $\vec{H}$
parallel to $\vec{b}$.

37

the magnetization measurement versus applied field along the three principal directions. The easy direction at 4.2K is the c axis with a spontaneous moment of about 3.74 μ_B/ErFe$_3$. If we attribute a moment of 9 μ_B to Er as in ErCo$_3$, the average moment of Fe is 1.75 μ_B.

As the temperature increases a sharp discontinuity in the magnetization at zero field along $\vec{c}$ is observed at T_{R_1} = 42K, Fig. 13. Above this
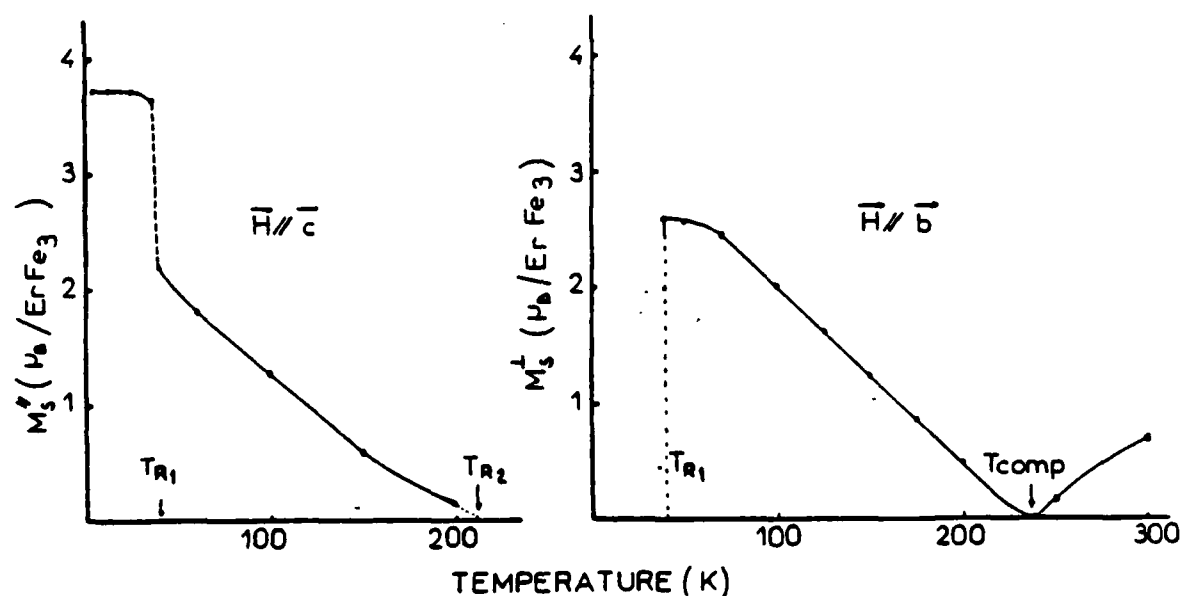
Fig. 13. Thermal variations of the spontaneous moment components $M_s^{||}$ and $M_s^{\perp}$ along $\vec{c}$ and $\vec{b}$.

temperature, the c axis is no longer the easy axis because a zero field magnetization is obtained along $\vec{a}$, $\vec{b}$, and $\vec{c}$. Above T_{R_2} = 210K the spontaneous component along the c axis is zero whereas those along $\vec{a}$ and $\vec{b}$ are equal. The (ab) plane perpendicular to $\vec{c}$, therefore, becomes the easy plane. Between T_{R_1} and T_{R_2}, a reorientation of the moments arises lending to a noncollinear structure, as evidenced by the sharp discontinuity of the angle of the

38

spontaneous moment with $\vec{c}$. Specifically at T_{R_1} there is a first order transition between two different magnetic phases, I and II. The transition can be induced below T_{R_1} by applying a field perpendicular to $\vec{c}$ and observed by the appearance of a discontinuity at a critical field, H_{C_1}. On the other hand, the inverse transition can be induced above T_{R_1} by application of a field parallel to $\vec{c}$ resulting in a critical field H_{C_2}. The thermal variation of these fields are shown in Figs. 14a and b and defines the stable regions of phases I and II as a function of field direction. In Fig. 12b the thermal variation of the basal component of magnetization above T_{R_2} = 210K corresponds to the thermal variation of the spontaneous magnetization. It becomes zero at T_{comp} = 235K, for which the magnetic moments of the Er atoms are equal and opposite to those of the Fe atoms.

(a)   TEMPERATURE   (b)
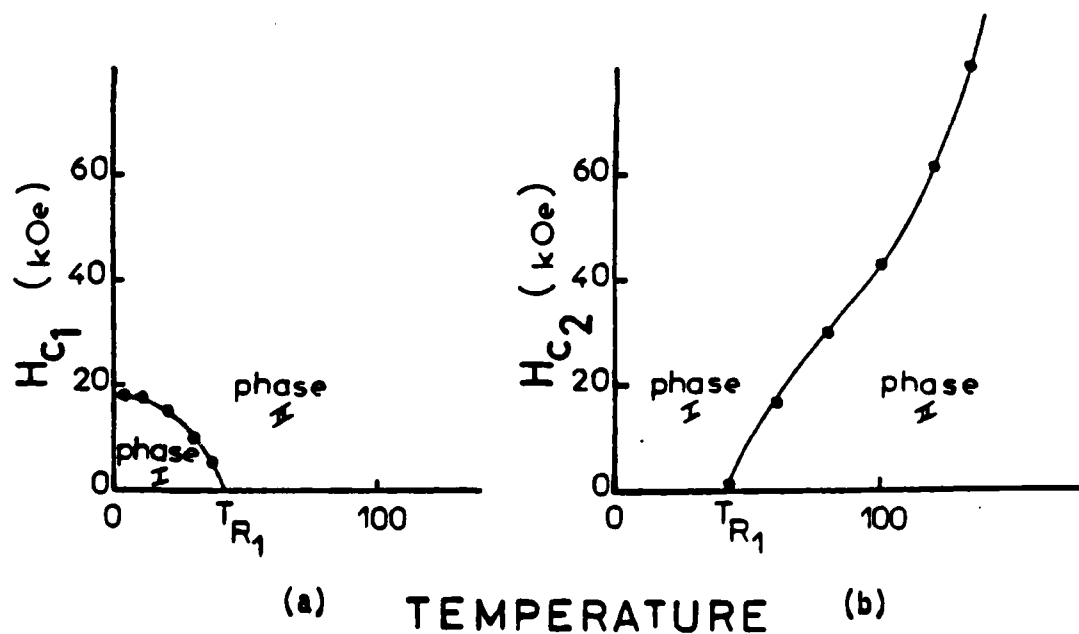
Fig. 14. Thermal variations of the critical fields along the direction of the applied field: (a) H_{C_1}, and (b) H_{C_2}.

Powder neutron diffraction data were collected at 4.2, 77, and 300K to establish the exact magnetic configurations of phases I and II, and of the stable phase III above 210K, Fig. 15. At 4.2K the magnetic (00ℓ) peaks are absent and, therefore, the easy axis is $\vec{c}$ in accord with the magnetization data. The refinement resulted in a weighted R factor of 2.5% for the moment values given in Table XIII. At 77K the 003 intensity is considerably increased, Fig. 15, the moments are no longer parallel to $\vec{c}$. As for ErNi$_3$, the best model is a noncollinear one in which the moments are in a plane containing the c axis. Their values and the angles, θ, which they make with the c axis are given in Table XIII. At 300K a collinear structure with the magnetic moments in the basal plane gives excellent agreement with the neutron data. The refinement results are in Table XIII.

Table XIII. Results of the refinement of neutron data for ErFe$_3$ at 4.2, 77, and 300K.

Atoms	4.2K		77K		300K	
	$M(\mu_B)$	θ	$M(\mu_B)$	θ	$M(\mu_B)$	θ
Er$_I$	9.6$\pm$0.5	0°	8.8$\pm$0.2	38$\pm$4°	3.6$\pm$0.3	90°
Er$_{II}$	8.9$\pm$0.3	0°	8.4$\pm$0.2	57$\pm$4°	4.1$\pm$0.2	90°
Fe	1.9$\pm$0.2	180°	1.9$\pm$0.1	236$\pm$4°	1.7$\pm$0.1	90°

It is evident that the magnetic behavior of the compounds of RFe$_3$ arises from the competition among the local anisotropies of the Fe atoms which, by reason of strong exchange interactions, leads to a total (net) anisotropy of iron favoring the plane perpendicular to the c axis.
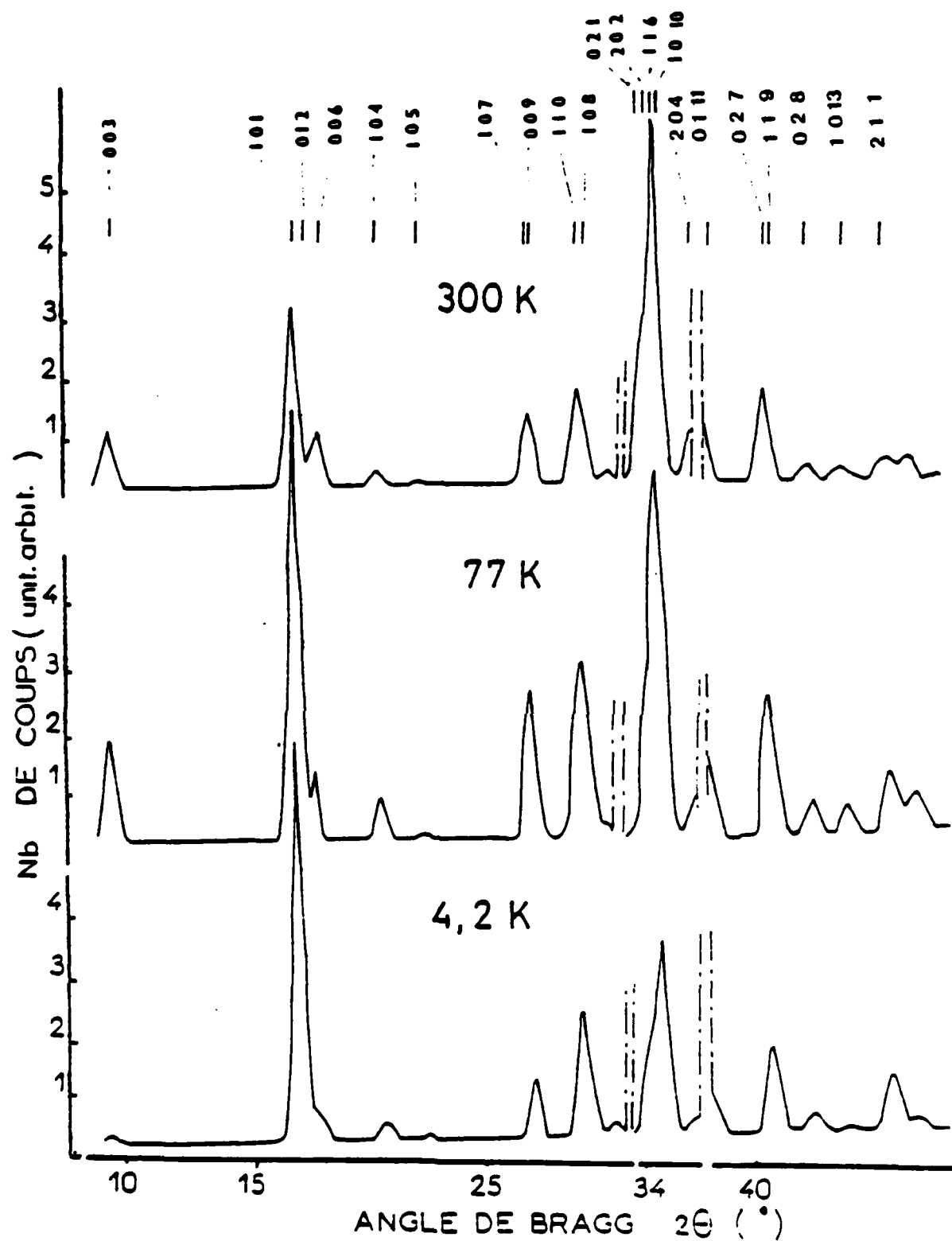
Fig. 15. Neutron diffraction data for $ErFe_3$ at 300, 77, and 4.2K.

III. LIST OF PUBLICATIONS

1. K. Hardman, J. J. Rhyne, and W. J. James, "Magnetic Structures of $Y_6(Fe_{1-x}Mn_x)_{23}$ Compounds", J. Appl. Phys., $\underline{52}$(3) (1981) 2049.

2. B. Kebe, W. J. James, J. Deportes, R. Lemaire, W. B. Yelon, and R. K. Day, "Neutron Diffraction and Magnetic Studies of $ErFe_3$", ibid, 2052.

3. B. Kebe, C. Crowder, W. J. James, J. Deportes, R. Lemaire, and W. B. Yelon, "Evidence for the Non-Collinearity of the Magnetic Structure of Er_6Mn_{23}", in G. J. McCarthy, J. J. Rhyne, and H. B. Silber (eds.) The Rare Earths in Modern Science and Technology, Vol. 3, Plenum, New York, 1982, p. 377.

4. B. Decrop, J. Deportes, B. Kebe, C. Crowder, W. J. James, and W. B. Yelon, "Magnetic Properties of ErM_3, M = (Ni, Fe, Co)", ibid, p. 361.

5. C. Crowder, B. Kebe, and W. J. James, "Magnetic and Structural Properties of $Y_6Mn_{23}D_{23}$", ibid, p. 473.

6. C. Crowder, W. J. James, and W. B. Yelon, "A Powder Neutron Diffraction Study of the $LaNi_{4.5}Al_{0.5}D_{4.5}$ Structure at 298 and 77K", J. Appl. Phys., $\underline{53}$(3) (1982) 2637.

7. C. Crowder, B. Kebe, W. J. James, and W. B. Yelon, "A Powder Neutron Diffraction Study of Antiferromagnetism in $Er_6Mn_{23}D_{23}$", A/P Conf. Proc., $\underline{89}$ (1982) 318.

8. W. J. James, T. G. D. van Schalkwyk, "The Effect of Stoichiometric Variations on the Magnetic Structure of Y_6Mn_{23}", J. Less-Common Met., $\underline{94}$ (1983) 221.

9. C. E. Crowder and W. J. James, "A Review of the Magnetic Structures and Properties of the R_6M_{23} Compounds and Their Hydrides", J. Less-Common Met., $\underline{95}$ (1983) 1.

10. K. Hardman-Rhyne, J. J. Rhyne, C. Crowder, and W. J. James, "Crystallographic and Magnetic Changes of $Y_6Mn_{23}D_{19}$ with Temperature in a Neutron Diffraction Study", ACA, UMC, Columbia, MO, March 14-18 (1983).

11. K. Hardman-Rhyne, J. J. Rhyne, E. Prince, C. Crowder, and W. J. James, "Magnetic and Crystallographic Structure of $Y_6Mn_{23}D_{23}$", Phys. Rev. B, 29(1) (1984) 416.

12. C. E. Crowder, "Powder Neutron Diffraction Studies of $Y_6Mn_{23}D_{23}$, $Er_6Mn_{23}D_{23}$ and $LiNi_4Al_{0.5}D_{4.5}$", Ph.D. Thesis, University of Missouri-Rolla (1982).

13. B. Kebe, "Contribution to the Study of the Magneto-crystalline Anisotropy of Rare Earth-3d Metal Compounds", Ph.D. Thesis, University of Grenoble, France, October (1983).

IV. PARTICIPATING SCIENTIFIC PERSONNEL

1. <u>Principal Investigator</u>: William J. James - Professor of Chemistry and Senior Investigator, Graduate Center for Materials Research.

2. <u>Co-Investigator</u>: Gary Long - Associate Professor of Chemistry.

3. <u>Graduate Research Assistants</u>:

   (1) Cyrus Crowder - Ph.D., Chemistry earned 1982

   (2) Baye Kebe - Ph.D., Physics earned 1983

   (3) Tamara Littlewood - candidate for Ph.D. in Chemistry

   (4) Dwayne Tharp - candidate for Ph.D. in Chemistry

*4. <u>Dr. R. Lemaire</u> - Néel Laboratory CNRS, Grenoble, France

   <u>Dr. J. Deportes</u> - Néel Laboratory CNRS, Grenoble, France

   <u>Dr. Y. C. Yang</u> - Physics Department, Peking University, Peoples Republic of China - Visiting Associate Professor, UMR 1981-82

   <u>Dr. W. B. Yelon</u> - University of Missouri Research Reactor, University of Missouri-Columbia, Columbia, MO

*Above did not receive salaries on project but did assist and interact with graduate students and principal investigator.

References

1. K. Hardman, W. J. James, and W. B. Yelon in G. J. McCarthy and J. J. Rhyne (eds.), <u>The Rare Earths in Modern Science and Technology</u>, Vol. 1, Plenum, New York, 1978, p. 403.

2. A. Delapalme, J. Deportes, R. Lemaire, K. Hardman, and W. J. James, J. Appl. Phys., <u>50</u> (1979) 1987.

3. H. M. Rietveld, J. Appl. Crystallogr., <u>2</u> (1969) 65.

4. H. R. Kirchmayer and W. Steiner, J. Phys. Suppl., <u>32</u> (1971) C1-665.

5. K. Hardman, W. J. James, G. J. Long, W. B. Yelon, and B. Kebe in G. J. McCarthy, J. J. Rhyne, and H. B. Silber (eds.), <u>The Rare Earths in Modern Science and Technology</u>, Vol. 2, Plenum, New York, 1980, p. 315.

6. G. J. Long, K. Hardman, and W. J. James, Solid State Comm., <u>34</u> (1980) 253.

7. A. Dworak, H. R. Kirchmayer, and H. Rauch, Z. angew. Phys., <u>6</u> (1968) 599.

8. G. Helscher and H. Rais, Phys. F: Metal Phys., <u>8</u>(3) (1978) 511.

9. K. H. J. Buschow and R. C. Sherwood, J. Appl. Phys., <u>49</u> (1978) 1480.

10. H. M. Rietveld, J. Appl. Cryst., <u>2</u> (1969) 65, modified by E. Prince, NBS, Washington, DC (1980).

11. K. Hardman, "Magnetic Structures of the R_6T_{23} Compounds of Rare Earth Transition Metal Intermetallics", Ph.D. Thesis, University of Missouri-Rolla (1979).

12. M. Commandre, D. Fruchart, A. Roualt, D. Sauvage, C. B. Shoemaker, and D. P. Shoemaker, J. de Physique, <u>40</u> (1979) 1-639.

13. K. H. J. Buschow and R. C. Sherwood, IEEE Trans. Magn., <u>13</u> (1977) 1571.

14. K. Hardman, J. J. Rhyne, H. K. Smith, and W. E. Wallace in G. J. McCarthy, J. J. Rhyne, and H. B. Silber (eds.), <u>The Rare Earths in Modern Science and Technology</u>, <u>3</u>, Plenum, New York, 1982, p. 477.

15. D. G. Westlake, J. Mater. Sci., 18 (1983) 605.

16. J. H. Wernick and S. Geller, Acta Cryst., 12 (1959) 662; A. E. Dwight, Trans. ASM, 53 (1961) 479.

17. A. E. Dwight, in G. J. McCarthy and J. J. Rhyne (eds.), The Rare Earths in Modern Science and Technology, Vol. 1, Plenum, New York, 1978, p. 325.

18. A. Percheron-Guegan, C. Lartigue, J. C. Achard, P. Germi, and F. Tasset, J. Less-Common Met., 74 (1980) 1; J. C. Achard, F. Givord, A. Percheron-Guegan, J. L. Soubeyroux, and F. Tasset, J. Phys. (Paris) Colloq., 5(40) (1979) 218.

19. P. Fischer, A. Furres, G. Busch, and L. Schlapbach, Helv. Phys. Acta, 50 (1977) 421.

20. V. V. Burnosheva, V. A. Yortys, N. V. Paduva, S. P. Solovlev, and K. N. Somenko, Dokl. Acad. Nauk SSSR, 238 (1978) 844.

21. W. E. Wallace, H. E. Flotow, and D. Ohlendorf, J. Less-Common Met., 79(1) (1981) 157.

22. R. G. Barnes, W. C. Harper, S. D. Nelson, D. K. Thome, and D. R. Torgeson, J. Less-Common Met., 49 (1976) 483.

23. T. K. Halstead, J. Solid State Chem., 11 (1974) 114.

24. M. H. Mendelsohn, D. M. Gruen, and A. E. Dwight, J. Less-Common Met., 63 (1979) 193.

25. E. Parthe and R. Lemaire, Acta Cryst., 331 (1975) 1879.

26. J. Yakinthos and J. Rossat-Mignod, Phys. Stat. Sol. (b), 50 (1972) 747.

27. R. Lemaire, Cobalt, 32 (1966) 132.

28. K. H. J. Buschow and A. S. van der Goot, Phys. Stat. Sol. (b), 35 (1969) 515.

END

FILMED

6-34

DTIC